Relative Importance of High-Latitude Local and Long-Range Transported Dust to Arctic Ice Nucleating Particles and Impacts on Arctic Mixed-Phase Clouds

Yang Shi[1], Xiaohong Liu[1], Mingxuan Wu[2], Xi Zhao[1], Ziming Ke[1], and Hunter Brown[1]

[1]Department of Atmospheric Sciences, Texas A&M University, College Station, TX, USA
[2]Atmospheric Sciences and Global Change Division, Pacific Northwest National Laboratory, Richland, WA, USA

Correspondence to: Xiaohong Liu (xiaohong.liu@tamu.edu)

Abstract. Dust particles, serving as ice nucleating particles (INPs), may impact the Arctic surface energy budget and regional climate by modulating the mixed-phase cloud properties and lifetime. In addition to long-range transport from low latitude deserts, dust particles in the Arctic can originate from local sources. However, the importance of high latitude dust (HLD) as a source of Arctic INPs (compared to low latitude dust (LLD)) and its effects on Arctic mixed-phase clouds are overlooked. In this study, we evaluate the contribution to Arctic dust loading and INP population from HLD and six LLD source regions by implementing a source-tagging technique for dust aerosols in version 1 of the US Department of Energy's Energy Exascale Earth System Model (E3SMv1). Our results show that HLD is responsible for 30.7% of the total dust burden in the Arctic, whereas LLD from Asia and North Africa contribute 44.2% and 24.2%, respectively. Due to its limited vertical transport as a result of stable boundary layers, HLD contributes more in the lower troposphere, especially in boreal summer and autumn when the HLD emissions are stronger. LLD from North Africa and East Asia dominates the dust loading in the upper troposphere with peak contributions in boreal spring and winter. The modeled INP concentrations show a better agreement with both ground and aircraft INP measurements in the Arctic when including HLD INPs. The HLD INPs are found to induce a net cooling effect (-0.24 W m^{-2} above 60°N) on the Arctic surface downwelling radiative flux by changing the cloud phase of the Arctic mixed-phase clouds. The magnitude of this cooling is larger than those induced by North African and East Asian dust (0.08 and -0.06 W m^{-2}, respectively), mainly due to different seasonalities of HLD and LLD. Uncertainties of this study are discussed, which highlights the importance of further constraining the HLD emissions.

1 Introduction

The Arctic has experienced long-term climate changes, including rapid warming and shrinking in sea ice extent. Arctic mixed-phase clouds (AMPCs), which occur frequently throughout the year, strongly impact the surface and atmospheric energy budget and are one of the main components driving the Arctic climate (Morrison et al., 2012; Shupe and Intrieri, 2004; Tan and Storelvmo, 2019). The AMPCs lifetime, properties, and radiative effects are closely connected to the primary ice formation process, as the formed ice crystals grow at the expense of cloud liquid droplets due to the lower saturation vapor pressure with respect to ice than that to liquid water (so-called Wegener-Bergeron-Findeisen process or, in short, WBF process; Liu et al., 2011; M. Zhang et al., 2019). Large ice crystals with higher fall speeds than liquid droplets can readily initiate precipitation and further deplete cloud liquid through the riming process. All these processes can also interact with each other nonlinearly and impact the phase partitioning of mixed-phase clouds (Tan and Storelvmo, 2016).

Primary ice formation in mixed-phase clouds only occurs heterogeneously with the aid of ice nucleating particles (INPs). According to Vali et al. (1985), the heterogeneous ice nucleation is classified into four different modes: through the collision of an INP particle with supercool liquid droplet (contact freezing), by an INP particle immersed in a liquid droplet (immersion freezing), when the INP particle also serves as a cloud condensation nucleus (condensation freezing), or by the direct deposition of water vapor to a dry INP particle (deposition nucleation). The immersion freezing is usually treated together with condensation freezing in models, as instruments cannot distinguish between them (Vali et al., 2015). This immersion/condensation freezing is generally thought to be the most important ice nucleation mode in the mixed-phase clouds (de Boer et al., 2011; Prenni et al., 2009; Westbrook and Illingworth, 2013). It remains a significant challenge to

56　characterize the INP types and concentrations, partially because only a very small fraction of

57　aerosols can serve as INPs (DeMott et al., 2010). This is especially the case for the clean

58　environment in the Arctic. Therefore, the potential sources and amounts of Arctic INPs are still

59　largely unknown.

60　　　Mineral dust aerosols are identified as one of the most important types of INPs in the

61　atmosphere due to their high ice nucleation efficiency (DeMott et al., 2003; Hoose and Möhler,

62　2012; Murray et al., 2012; Atkinson et al., 2013) and their abundance in the atmosphere (Kinne

63　et al., 2006). They are mainly emitted from arid and semi-arid regions located at low- to mid-

64　latitudes, such as North Africa, the Middle East, and Asia. Observational studies found that LLD

65　can be transported to the Arctic (Bory et al., 2003; VanCuren et al., 2012; Huang et al., 2015)

66　and act as a key contributor to the Arctic INP population (Si et al., 2019). A modelling study also

67　suggested that low latitude dust (LLD) has a large contribution to dust concentrations in the

68　upper troposphere of the Arctic (Groot Zwaaftink et al., 2016), since LLD is usually lifted by

69　convection and topography and then transported poleward following slantwise isentropes. This

70　finding confirms the potential of LLD to serve as INPs in AMPCs. The impact of LLD INPs on

71　clouds was further investigated by Shi and Liu (2019), who found that LLD INPs induce a net

72　cooling cloud radiative effect in the Arctic, due to their impacts on cloud water path and cloud

73　fraction.

74　　　Although LLD has attracted much of the attention in the past, it is recognized that 2–3% of the

75　global dust emission is produced by local Arctic sources above 50°N (Bullard et al., 2016),

76　which include Iceland (Arnalds et al., 2016; Dagsson-Waldhauserova et al., 2014; Prospero et al.,

77　2012), Svalbard (Dörnbrack et al., 2010), Alaska (Crusius et al., 2011), and Greenland (Bullard

78　and Austin, 2011). Groot Zwaaftink et al. (2016) found that high latitude dust (HLD) contributes

79   27% of the total dust burden in the Arctic. Different from LLD, most of the emitted HLD is

80   restricted at the lower altitudes in the Arctic, because of the stratified atmosphere in the cold

81   environment (Bullard, 2017; Groot Zwaaftink et al., 2016).

82   It is also noted that HLD is likely an important source to the observed INPs in the Arctic,

83   especially during the warm seasons. For example, Irish et al. (2019) suggested that mineral dust

84   from Arctic bare lands (likely eastern Greenland or north-western continental Canada) is an

85   important contributor to the INP population in the Canadian Arctic marine boundary layer during

86   summer 2014. Attempts have been made to quantify the ice nucleating ability of HLD.

87   Paramonov et al. (2018) found that the Icelandic glaciogenic silt had a similar ice nucleating

88   ability as LLD at temperatures below -30 °C. Similarly, Sanchez-Marroquin et al. (2020)

89   suggested that the ice nucleating ability of aircraft-collected Icelandic dust samples is slightly

90   lower but comparable with that of the LLD. Some other studies also noticed that HLD can act as

91   efficient INPs at warm temperatures. As early as the 1950s, the airborne dry dust particles from

92   permafrost ground at Thule, Greenland, were found to nucleate ice at temperatures as warm as -5

93   °C (Fenn and Weickmann, 1959). This is corroborated by a more recent study which investigated

94   the glacial outwash sediments in Svalbard and ascribed the remarkably high ice nucleating

95   ability to the presence of soil organic matter (Tobo et al., 2019).

96   Despite their potential importance, HLD sources are largely underestimated or even omitted in

97   global models (Zender et al., 2003). Fan (2013) noticed that the autumn peak in measured

98   surface dust concentrations at Alert was underestimated by the model, likely due to a lack of

99   local dust emission. Similarly, Shi and Liu (2019) also mentioned that the distinction of

100   simulated and satellite retrieved dust vertical extinction in the Arctic became larger near the

101   surface.

102   In this study, we account for the HLD dust emission by replacing the default dust emission

103   scheme (Zender et al., 2003) with the Kok et al. (2014a, b) scheme in the Energy Exascale Earth

104   System Model version 1 (E3SMv1). We further track explicitly the dust aerosols emitted from

105   the Arctic (HLD) and six major LLD sources using a newly developed source-tagging technique

106   in E3SMv1. The objectives of this study are to (1) examine the source attribution of the Arctic

107   dust aerosols in the planetary boundary layer and in the free troposphere; (2) examine the

108   contribution of dust from various sources to the Arctic dust INPs; and (3) quantify the

109   subsequent influence of dust INPs from various sources on the Arctic mixed-phase cloud

110   radiative effects. We are particularly interested in the relative importance of local HLD versus

111   long-range transported LLD.

112   The paper is organized as follows. The E3SMv1 model and experiments setup are introduced

113   in Section 2. Section 3 presents model results and comparisons with observations. The

114   uncertainties are discussed in Section 4, and Section 5 summarizes the results.

115   **2 Methods**

116   **2.1 Model description and experiment setup**

117   Experiments in this study are performed using the atmosphere component (EAMv1) of the U.S.

118   Department of Energy (DOE) E3SMv1 model (Rasch et al., 2019). The model predicts number

119   and mass mixing ratios of seven aerosol species (i.e., mineral dust, black carbon (BC), primary

120   organic aerosol, secondary organic aerosol, sulfate, sea salt, and marine organic aerosol (MOA))

121   through a four-mode version of modal aerosol module (MAM4) (Liu et al., 2016; Wang et al.,

122   2020). The four aerosol modes are Aitken, accumulation, coarse, and primary-carbon modes,

123   while dust aerosols are carried in accumulation and coarse modes. Aerosol optical properties in

124   each mode is parameterized following Ghan and Zaveri (2007). The dust optics used in this study

125   are updated according to Albani et al. (2014).

126   EAMv1 includes a two-moment stratiform cloud microphysics scheme (MG2) (Gettelman and

127   Morrison, 2015). We note the WBF process rate in EAMv1 is tuned down by a factor of 10,

128   which results in more prevalent supercooled liquid water clouds in high latitudes than

129   observations and many other global climate models (Y. Zhang et al., 2019; Zhang et al., 2020).

130   In addition, the Cloud Layers Unified By Binormals (CLUBB) parameterization (Bogenschutz et

131   al., 2013; Golaz and Larson, 2002; Larson et al., 2002) is used to unify the treatments of

132   planetary boundary layer turbulence, shallow convection, and cloud macrophysics. Deep

133   convection is treated by the Zhang and McFarlane (1995) scheme.

134   In EAMv1, the heterogeneous ice nucleation in mixed-phase clouds follows the classical

135   nucleation theory (CNT) (Hoose et al., 2010; Y. Wang et al., 2014). CNT holds the stochastic

136   hypothesis, which treats the ice nucleation process as a function of time.

137   Immersion/condensation, contact, and deposition nucleation on dust and BC are treated in the

138   CNT scheme. More details about CNT parameterization are provided in Text S2.1 in the

139   Supplement.

140   The experiments we conducted for this study are shown in Table 1. For the control experiment

141   (hereafter CTRL), the EAMv1 was integrated from July 2006 to the end of 2011 at 1° horizontal

142   resolution and 72 vertical layers. The first six months of the experiment were treated as model

143   spin-up and the last five-year results were used in analyses. The horizontal wind components

144   were nudged to the MERRA2 meteorology with a relaxation timescale of 6 hours (Zhang et al.,

145   2014). In addition to CTRL, we conducted three sensitivity experiments to investigate the INP

146   effect of dust from major source regions. In these sensitivity experiments, heterogeneous ice

147   nucleation in the mixed-phase clouds by dust from local Arctic sources, North Africa, and East

148   Asia is turned off (i.e., noArc, noNAf, and noEAs, respectively). The other settings of these three

149   experiments are identical to CTRL. Analyses related to the sensitivity experiments are provided

150   in Section 3.4.

151   **2.2 Dust emission parameterization and source-tagging technique**

152   Dust emission in the default EAMv1 is parameterized following Zender et al. (2003) (Z03),

153   which uses semi-empirical dust source functions to address the spatial variability in soil

154   erodibility. The HLD emission is omitted in the Z03 scheme, since it was thought to be dubious

155   (Zender et al., 2003). In this study, we replaced the Z03 scheme with another dust emission

156   parameterization (Kok et al., 2014a, b) (K14) that avoids using a source function (see more

157   details about K14 in Text S1). The K14 scheme is able to produce the HLD emission over

158   Iceland, the Greenland coast, Canada, Svalbard, and North Eurasia (Figure 1a). Furthermore, to

159   address the overestimation in dust emission in clay size (< 2 μm diameter) (Kok et al., 2017), we

160   changed the size distribution of emitted dust particles from Z03 to that based on the brittle

161   fragmentation theory (Kok, 2011). 1.1% of the total dust mass is emitted to the accumulation

162   mode and 98.9% of that is emitted to the coarse mode based on the brittle fragmentation theory,

163   whereas the fractions are 3.2% and 96.8%, respectively in Z03.

164   To quantify the source attribution of dust, we implemented a dust source-tagging technique in

165   EAMv1. This modeling tool was previously applied to BC (H. Wang et al., 2014; Yang et al.,

166   2017b), sulfate (Yang et al., 2017a), and primary organic aerosol (Yang et al., 2018) in the

167   Community Atmosphere Model version 5 (CAM5). In this method, dust emission fluxes from

168   different sources are assigned to separate tracers and transport independently, so that dust

169   originating from different sources can be tracked and tuned separately in a single model

8

experiment. As shown in Figure 1a, dust emissions from 7 source regions are tagged: Arctic (Arc; above 60°N, HLD source), North America (NAm), North Africa (NAf), Central Asia (CAs), Middle East and South Asia (MSA), East Asia (EAs), and rest of the world (RoW). The Arctic source is further divided into four sub-sources: Alaska (Ala), North Canada (NCa), Greenland and Iceland (GrI), and North Eurasia (NEu) (Figure S1), which are used in the analysis of INP sources in Section 3.3. RoW represents the three major dust sources in the Southern Hemisphere (South America, South Africa, and Australia), along with very low emissions from Europe and the Antarctic.

The global dust emission for CTRL is 5640 Tg yr^{-1}, which is tuned so that the global average dust aerosol optical depth (DOD) is 0.031. This is within the range of the observational estimate (0.030±0.005) by Ridley et al. (2016). To maintain the magnitude of the global averaged DOD, our tuned global dust emission exceeds the range of the AeroCom (Aerosol Comparisons between Observations and Models) models (500 to 4400 Tg yr^{-1}; Huneeus et al., 2011), likely due to a short lifetime caused by too strong dust dry deposition at the bottom layer near the dust source regions in EAMv1 (Wu et al., 2020). It is also about 2000 Tg yr^{-1} higher than the previous EAMv1 studies (Shi and Liu, 2019; Wu et al., 2020), because we distribute less dust mass into the accumulation mode and more dust mass into the coarse mode based on Kok (2011). The HLD emission is further tuned up by 10 times so that it accounts for 2.6% (144 Tg yr^{-1}) of the global dust emission (Figure 1b), which is comparable with the recent estimates of 2-3% above 50°N by Bullard et al. (2016) and of 3% above 60°N by Groot Zwaaftink et al. (2016). The majority of global dust emission is contributed from North Africa (51.9%, 2929 Tg yr^{-1}) and Asia (37.7%, 2124 Tg yr^{-1}), with Asian emissions composed of MSA (20.2%, 1140 Tg yr^{-1}), EAs (10.9%, 613 Tg yr^{-1}), and CAs (6.6%, 371 Tg yr^{-1}). NAm has a weak dust emission of 33.4 Tg

193   yr^{-1} that only contributes 0.6% to the global emission, while the RoW has a combined

194   contribution of 7.3% (410 Tg yr^{-1}). In addition, the seasonal variations between HLD and LLD

195   emissions are different - the HLD (Arctic) source is more active in late summer and autumn,

196   while the LLD sources (e.g., NAf, MSA, EAs) peak in spring and early summer (Figure 1c).

197   **3 Result**

198   **3.1 Model validation**

199   To evaluate the model performance in simulating the dust cycle, we compare the model

200   predictions with measured aerosol optical depth (AOD), dust surface concentrations, and dust

201   deposition fluxes from global observation networks (Figure 2). We select and process the level

202   2.0 AOD data (2007-2011) at 40 "dust-dominated" AErosol RObotic NETwork (AERONET;

203   Holben et al., 1998) stations following Kok et al. (2014b). We note that the AERONET AOD

204   measurements are biased towards clear-sky conditions due to the cloud-screening procedure

205   (Smirnov et al., 2000). For dust surface concentrations, we use the same measurements at 22

206   sites, which Huneeus et al. (2011) used for the AeroCom comparison, and further extend the

207   dataset with measurements at three high latitude stations: Heimaey (Prospero et al., 2012), Alert

208   (Sirois and Barrie, 1999), and Trapper Creek (Interagency Monitoring of Protected Visual

209   Environments; IMPROVE). It is noted that the measurements at Trapper Creek only include dust

210   particles smaller than 2.5 μm and are only compared with simulated dust concentrations at the

211   same size range. All other concentration measurements capture dust particles below 40 μm and

212   are compared with simulated dust over the whole size range (< 10 μm). The dust deposition

213   fluxes dataset, which including 84 stations, is also the same as Huneeus et al. (2011). The

214   locations of the observation network are shown in Figure 2d, with the AOD data taken close to

215   source regions and the dust surface concentrations and deposition fluxes measured at relatively

216   remote regions. The Pearson correlation coefficient (r) are provided for each comparison. We

217   note that the comparisons are subject to representative biases caused by comparing an

218   observational station with a global model grid point (with a horizontal resolution of ~ 100 km).

219   The comparisons of dust concentration and deposition flux also have systematic errors because

220   the measurements were for a different time period than that of the model simulation.

221   In general, the three comparisons indicate that our CTRL simulation is capable of capturing

222   the global dust cycle in both near the source and remote regions. As shown in Figure 2a, the

223   modeled AOD is within a factor of two of the observations over most of the stations. The

224   correlation of the AOD comparison is 0.73, which is comparable to the best performing

225   simulation (r = 0.72) in Kok et al. (2014b). Our model also does a fairly good job in simulating

226   the dust surface concentrations (Figure 2b) and produces a correlation coefficient of 0.84. For the

227   three high latitude sites, the model shows moderate underestimation at Heimaey and Trapper

228   Creek and large positive bias at Alert (see discussion below). The correlation coefficient for

229   simulated dust deposition fluxes (r = 0.48) is also within the range of the AeroCom comparisons

230   (0.08 to 0.84) in Huneeus et al. (2011). The model results over most of the sites are within one

231   order of magnitude difference, except at the polar regions. In particular, the model overestimates

232   the dust deposition flux in Greenland (red triangles in Figure 2c and 2d) by around two orders of

233   magnitude, likely due to too strong local emissions simulated near the coast of Greenland (Figure

234   1a).

235   The seasonal cycle of dust surface concentrations at the three Arctic stations (Heimaey, Alert,

236   and Trapper Creek) are shown in Figure 3, along with the contribution from seven tagged

237   sources. The simulated dust concentrations at Heimaey are dominated by HLD and agree well

238   with the observation in late summer and autumn (Figure 3a). Its annual-averaged low bias shown

239   in Figure 2b mainly comes from the springtime, when Prospero et al. (2012) found the observed

240   dust are related to dust storms in Iceland, indicating a possible underestimation in the simulated

241   Icelandic dust during this time. The HLD also dominates the surface dust concentrations at Alert

242   (Figure 3b), leading to a large overestimation from June to August in our simulation, which

243   possibly implies a high bias and wrong seasonal cycle of HLD emission over Greenland and

244   North Canada. The Trapper Creek station is instead dominated by LLD from East Asia and

245   shows an underestimation for most of the year. It is noted that we only include fine dust

246   (diameter < 2.5 μm) for the comparison at Trapper Creek. Larger size range is likely to be more

247   influenced by HLD sources. The low bias here, especially that during the autumn, can be related

248   to the missing of local emissions from the coast of Southern Alaska (Figure 1a) that occurs most

249   frequently in autumn (Crusius et al., 2011). An underestimation of the transport from Saharan

250   dust may also contribute slightly, as the influence from Saharan dust is found during mid-May at

251   Trapper Creek (Breider et al., 2014).

252   The simulated Arctic dust vertical profiles are also compared with the measured dust

253   concentrations during the Arctic Research of the Composition of the Troposphere from Aircraft

254   and Satellites (ARCTAS) flight campaign (Figure 4) (Jacob et al., 2010). The ARCTAS

255   campaign was conducted over the North American Arctic in April and July 2008. The simulated

256   profiles are averaged over the regions where the aircraft flew, in accordance with Groot

257   Zwaaftink et al. (2016). In April, the model does a good job in capturing the Arctic dust vertical

258   profiles (Figure 4a). However, in July, the model underestimates dust by a factor of 2 to 5

259   between 3 and 10 km (Figure 4b). It also shows an overestimation near the surface in July, which

260   agrees   with   the   surface   concentrations   comparison   at   Alert   station   (Figure   3b).   The

261   underestimation in the upper troposphere and overestimation near the surface likely imply a too

262   weak vertical transport of HLD in the North American Arctic in summertime. The high bias in

263   the upper troposphere may also be related to an underrepresentation of LLD transport.

264   Finally, we evaluate the simulated dust extinction against the Cloud-Aerosol Lidar and

265   Infrared Pathfinder Satellite Observation (CALIPSO) retrieval (Luo et al., 2015a, b), which

266   includes nighttime dust extinction for the period of 2007 to 2009. The Luo et al. (2015a, b) data

267   set has improvements in dust separation from other aerosol types and thin dust layer detection in

268   the Arctic than the standard CALIPSO product (Winker et al., 2013). To make an apple-to-apple

269   comparison, the modeled dust extinction is sampled along the CALIPSO tracks and screened by

270   cloud fraction (Wu et al., 2020). For this comparison, we only use the first three years (2007 to

271   2009) of the CTRL simulation to be consistent with the observation period. Overall, the model

272   does a good job in capturing the Arctic dust extinction vertical profiles (Figure 5). We notice that

273   the simulated dust extinction is lower than CALIPSO retrievals at the upper troposphere in

274   summer, which agrees with the ARCTAS comparisons. The simulated dust extinction also shows

275   a consistent underestimation in springtime (MAM) and a near surface underestimation in

276   wintertime (MAM). Since the Arctic is mostly covered by ice and snow in these two seasons, the

277   impacts of HLD are expected to be limited and the low biases are most likely due to the

278   underprediction of LLD transport. The near surface underestimation in DJF may indicate a too

279   weak LLD transport in the lower troposphere (e.g., the transport of dust emitted from Central

280   Asia; see Figure 7 and the corresponding discussions in Section 3.2). Moreover, the HLD has a

281   large contribution in the lower troposphere in boreal summer and autumn, which is consistent

282   with its strong emission at that time. In contrast, LLD plays a more dominant role in the upper

13

283   troposphere, where African dust contributes the most in the springtime and East Asian dust has a

284   larger contribution in the other seasons.

285   **3.2 Arctic dust mass source attribution**

286   Table 2 summarizes the relative contributions from individual sources to the total Arctic dust

287   burden. The transport pathways can be identified from the dust burden spatial distribution for

288   each source in Figure 6, while the relative contribution of each source to the total dust burden is

289   shown in Figure S2. We also calculate the regional burden efficiency for each source (Table S1),

290   which is defined as the mean contribution to the Arctic dust column burden divided by the

291   corresponding dust emission (H. Wang et al., 2014). This metric represents the sensitivity of

292   Arctic dust loading to per unit change of dust emission from each source (i.e., the poleward

293   transport efficiency of each source).

294   Our model results suggest that the HLD (Arc) is the largest contributor (30.7%) to the annual

295   mean Arctic dust burden among all the tagged sources. As shown in Figure 6a and Figure S2a,

296   the local dust is confined within the high latitudes, with the higher amounts and higher

297   contributions to the total dust burden near the sources in North Canada, coast of Greenland, and

298   Iceland. The interior of the Greenland ice sheet, with its higher elevations, is more influenced by

299   LLD from North Africa and East Asia than HLD (Figure S2c and S2f). This is due to the weak

300   vertical transport of local emissions in the Arctic (see more discussions below).

301   On the other hand, all LLD sources are responsible for 69.3% of the dust loading in the Arctic,

302   with considerable contributions from North Africa (24.2%) and Asia (in total 44.2%; EAs:

303   19.9%, MSA: 11.5%, CAs: 12.8%), and minor contributions from NAm (0.1%) and RoW (nearly

304   0). The North African dust is primarily transported westward to the Atlantic and southward to

305   Sahel, with a smaller fraction transported directly northward or northeastward across the Eurasia

306   to the Arctic (Figure 6c; Shao et al., 2011). The westward trajectory can also bring dust to the

307   Arctic through the Azores high (e.g., VauCuren et al., 2012), but this pathway is not clearly seen

308   on Figure 6c likely due to the strong wet removal process over the North Atlantic. As evident by

309   the low transport efficiency in Table S1, the significant contribution of the North African dust to

310   the Arctic dust burden is mainly due to its massive emission. However, this is not the case for

311   EAs. The East Asian dust is first lifted vertically by topography and convection (Shao et al.,

312   2011) and is widely spread over the Northern Hemisphere mid- and high-latitude regions through

313   the westerly flow in the upper troposphere (Figure 6f). The high elevation of East Asian dust

314   plumes results in weaker removal processes and thus an efficient poleward transport. As shown

315   in Table S1, the annual transport efficiency of the East Asian dust is relatively high among the

316   LLD sources, which is nearly three times larger than that of the North African dust. The

317   poleward transport of dust from CAs and MSA both takes the pathway across Siberia (Figure 6d

318   and 6e). The transport efficiency of the CAs dust is two times higher than that of the MSA dust

319   (Table S1). This is attributed to CAs being closer to the Arctic and having less southward dust

320   transport than MSA. Overall, the LLD from North Africa and Asia contributes more to the

321   Eurasia and Pacific sector of the Arctic (Figures S2c to S2f). The impact of NAm dust is limited

322   by its weak emission (Figure 6b), while dust emitted in the Southern Hemisphere (RoW) can

323   hardly pass the equator (Figure 6g).

324   Earlier modeling studies (Breider et al., 2014; Groot Zwaaftink et al., 2016; Luo et al., 2003;

325   Tanaka and Chiba, 2006) also quantify the relative contributions of dust from various regions to

326   the Arctic dust loading. Among these studies, only Groot Zwaaftink et al. (2016) includes HLD.

327   Our estimate about the HLD percent contribution is close to that from their study (27%). For

328   LLD, our conclusion about the dominant role of African and Asian dust to the Arctic dust burden

15

329   is also corroborated by these previous studies. However, the relative importance of African and

330   Asian dust is uncertain. Based on our results, the Asian dust is responsible for 65% of the LLD

331   transport to the Arctic, while the African dust only contributes 35%. Other studies find that 50%

332   (Groot Zwaaftink et al., 2016; Luo et al., 2003; Tanaka and Chiba, 2006) to as much as 65%

333   (Breider et al., 2014) of the LLD in the Arctic is attributed to North Africa. These discrepancies

334   may be explained by the different dust emission and scavenging, dust size distribution,

335   meteorological fields, and/or time periods for the model simulation. For example, North Africa

336   dust in our study contributes slightly less (51.9%) to the global dust emission than the other

337   studies (from 57% to 67%). Isotopic analysis (Bory et al., 2002, 2003) and case studies (Huang

338   et al., 2015; Stone et al., 2005; VanCuren et al., 2012) have proved that both Asian and African

339   dust can be transported to the Arctic. However, it remains unclear which of them contributes

340   more to the Arctic dust loading due to the limited observational constraints.

341   HLD and LLD source regions also have very distinct vertical distributions in the Arctic.

342   Figures 7a and 7b show the annual mean vertical profiles of Arctic dust concentrations from

343   various sources and their percentage contributions, respectively. The Arctic dust in the lower

344   atmosphere is dominated by the local source. HLD accounts for more than 30% of the Arctic

345   dust concentrations below 800 hPa, with up to 85% contribution near the surface. However, the

346   HLD contribution decreases rapidly with height and is less than 10% above 700 hPa. This is

347   because the lower troposphere of the Arctic is more stratified than the mid- and low latitudes,

348   which suppresses the vertical transport of HLD. The lower tropospheric stability (LTS) from the

349   CTRL simulation and comparison with the MERRA2 reanalysis data are shown in Figure S3.

350   The weak HLD vertical transport in the Arctic is also reported by previous studies (Groot

351   Zwaaftink et al., 2016, Baddock et al., 2017; Bullard, 2017). Moreover, the LTS over the Arctic

352 sea ice is much larger than that over open ocean surface (Schweiger et al., 2008), which may lead

353 to a stronger vertical transport of HLD over open waters. This suggests that the vertical transport

354 of HLD may change with the sea ice reduction in a warming future.

355 In contrast, LLD has a higher contribution in the mid- and upper troposphere than near the

356 surface. Such a vertical distribution of LLD is consistent with Stohl (2006) and Groot Zwaaftink

357 et al. (2016). As Stohl (2006) found, aerosols originating from the warm subtropics are

358 transported poleward following the uplifted isentropes and the Arctic lower atmosphere is

359 dominated by the near-impenetrable cold polar dome. Therefore, there is a slantwise lifting of

360 low latitude aerosols during their poleward transport. NAf and EAs are the two key contributors

361 to the Arctic dust vertical concentrations, each of which contributes up to one third of the total

362 dust concentrations above 700 hPa. Dust emission from MSA also has a moderate contribution

363 (15-20%) that increases gradually with height, while the contribution from CAs peaks at 700 to

364 800 hPa, indicating a lower altitude transport pathway than the EAs and MSA dust.

365 In addition, the Arctic dust undergoes a strong seasonal cycle (Table 2 and Figures 7c-j).

366 Because of the strong local emissions (Figure 1c), about half of the Arctic dust burden in

367 summer and autumn come from HLD, with more than 50% contribution of Arctic dust

368 concentrations below 850 hPa in these two seasons. In contrast, LLD plays a dominant role in

369 spring and winter. The North African dust has the largest contribution in spring, which accounts

370 for about 45% of the total dust concentrations above 700 hPa. The East Asian dust is more

371 important in the other three seasons. Due to its high emission height, the relative contribution

372 from EAs tends to increase with height and reaches 30% to 50% of the total dust concentration

373 above 500 hPa in summer, spring, and winter.

3.3 Immersion freezing on dust in the AMPCs

We are particularly interested in the contribution of various dust sources to the Arctic INP populations. Therefore, we compare the simulated INP concentrations with nine Arctic field measurements, which are summarized in Table 3. The modeled dust INP concentrations are diagnosed from monthly averaged aerosol properties using the default CNT scheme and two empirical ice nucleation parameterizations, DeMott et al. (2015; hereafter as D15) and Sanchez-Marroquin et al. (2020; hereafter as SM20). The D15 parameterization, which is representative of Saharan and Asian desert dust, relates dust INP number concentrations to the number concentration of dust particles larger than 0.5 μm diameter and is found to produce the most reasonable LLD INP concentrations in EAMv1 (Shi and Liu, 2019). CNT and D15 are applied to LLD only and all the dust aerosols (LLD and HLD) in Figures 8a-b and Figures 8d-e, respectively. The SM20 parameterization, which is derived for the HLD Icelandic dust, describes the dust INP number concentrations as a function of surface active site density and total dust surface area. Considering the possibly different ice nucleation ability between HLD and LLD, we only applied the SM20 parameterization to HLD and the CNT and D15 parameterizations are still applied to LLD in Figures 8c and 8f, respectively. To account for the contributions from other aerosol types, we also calculate the INP concentrations from BC (Fig. 8g) and sea spray aerosol (SSA; includes MOA and sea salt) (Fig. 8h) following Schill et al. (2020; hereafter as Sc20) and McCluskey et al. (2018; hereafter as M18), respectively. More details about the ice nucleation parameterizations are provided in Text S2. We discuss the choice of dust ice nucleation schemes in Text S2.6 in the Supplement.

Overall, only including LLD as INPs results in up to four orders of magnitude underprediction compared to observations (Figures 8a and 8d), while taking into account the contribution from

397   HLD greatly improves the model performance by increasing the simulated dust INP

398   concentrations (Figures 8b, 8c, 8e, and 8f). The CNT parameterization produces 5 to 10 times

399   more INP concentrations than the other two schemes at moderately cold temperatures (-22 to -

400   28℃), while it has a significant underestimation of observed INP concentrations at warm

401   temperatures (T > -18°C) (also see Figure S4). D15 and SM20 agree well with each other in

402   simulating HLD INPs, with SM20 producing slightly higher results than D15. Our modeling

403   results also indicate that BC and SSA have much less contributions to INP than dust in all the

404   nine field campaigns (Figure 8g and 8h).

405   A detailed analysis of sources of the INPs for the nine datasets based on modeling analyses

406   and the corresponding observations in the literature are provided in Table 3. Modeling results

407   indicate that HLD has larger contributions to the INPs for the campaigns conducted in summer

408   and autumn than spring, in agreement with the observations. Also, ground-based measurements

409   are more influenced by the nearby HLD sources, while LLD from EAs and NAf contributes

410   more to the aircraft measurements.

411   Our modeling analyses about the INP sources agree well with the observational studies at

412   Alert in spring 2016 and near Iceland in autumn 2014 (symbol "C" and "I" in Figure 8,

413   respectively), while the model underestimates the observed INP concentrations in both cases.

414   The low bias in dataset C indicates an underprediction in the long-range transport of Asian dust

415   to the Arctic surface in springtime. The underestimation in dataset I is more likely due to the fact

416   that some of the aircraft measurements were taken inside the Icelandic dust plumes (Sanchez-

417   Marroquin et al., 2020), which cannot be resolved by the monthly mean model output and the

418   coarse model horizontal resolution (1°). Such uncertainties exist in all the model-observation

419   comparisons.

420   Some other comparisons in INP sources reveal the lack of marine and carbonaceous INPs in

421   the model. The model results show a dominance of dust INPs in spring 2017 at Zeppelin and

422   Oliktok Point (symbol "D" and "E" in Figure 8) and in Autumn 2004 at Utqiaġvik (symbol "H"

423   in Figure 8), while the observational studies suggested the importance of marine sources at the

424   first two locations and of carbonaceous aerosols at Utqiaġvik. Therefore, it is likely that the

425   model underestimates the contribution of MOA (Wilson et al., 2015; Zhao et al., 2021a) and

426   does not account for terrestrial biogenic INPs (Creamean et al., 2020) due to the lack of

427   treatments in the model. In addition, both D15 and SM20 schemes cannot represent the high ice

428   nucleating ability of HLD at warm temperatures at Zeppelin in summer 2016 (symbol "G" in

429   Figure 8), which is attributed to soil organic matter by Tobo et al. (2019). When these organics

430   are taken into account in the model, model overestimation for site G will get even worse,

431   implying an overestimation of surface dust concentrations and/or HLD dust emission at Svalbard

432   in the summertime. In summary, the model's INP biases in the Arctic are likely due to biases in

433   the simulated aerosol fields (e.g., dust, MOA, and BC) and uncertainties in current ice nucleation

434   parameterizations or missing representations of other INP sources (e.g., terrestrial biogenic

435   aerosols).

436   In addition, it is noted that we do not explicitly represent the potential ice nucleation ability

437   differences in freshly emitted HLD and long-range transported LLD caused by the chemical

438   aging and coating of dust (Boose et al., 2016). However, D15 and SM20 may already take the

439   aging effect into account implicitly. Because D15 includes Saharan and Asian dust data collected

440   over Pacific Ocean basin and US Virgin Islands, respectively, which are far away from the

441   corresponding LLD sources, while SM20 are derived from freshly emitted Icelandic dust, which

442   is subjected to less aging processes.

443   The comparisons above are based on INP concentrations at a given temperature set by the INP

444   instruments, which reflects the potential INP populations under ambient aerosol conditions. Next,

445   we examine the immersion freezing rate of dust originating from the seven tagged sources

446   (Figure 9) to evaluate the influences of HLD and LLD on ice nucleation processes in mixed-

447   phase clouds. It is noted that the immersion freezing rate here is calculated online in the model

448   using the ambient temperature and the default CNT ice nucleation parameterization.

449   Compared with its contribution to the dust burdens, the contribution of the HLD to the annual

450   mean mixed-phase cloud immersion freezing rate is relatively small (~10% below 600 hPa)

451   (Figure 9a). This is because the HLD is mainly located in the lower troposphere and not a lot of

452   HLD can reach the mixed-phase cloud levels (or the freezing level), especially under the case

453   that the HLD tends to be more prevalent in the warm seasons (see more discussion below).

454   Among the LLD sources, North African dust (Figure 9c) and East Asian dust (Figure 9f) are the

455   two major contributors, both of which are responsible for more than 20% of the annual mean

456   immersion freezing rate in the mixed-phase clouds. Consistent with the vertical distribution of

457   dust concentrations, the North African dust has its maximum contribution (30-40%) at around

458   500 hPa, while the East Asian dust plays a more important role at higher altitudes (above 400

459   hPa). Dust from Central Asia also has a moderate contribution (~20%) to the immersion freezing

460   rate in the Arctic (Figure 9d).

461   Considering the different seasonality of HLD and LLD in the Arctic, we next investigate the

462   seasonal variations of the immersion freezing rate in the Arctic mixed-phase clouds from HLD

463   and two dominating LLD sources (NAf and EAs) (Figure 10). HLD has the largest contribution

464   to the Arctic immersion freezing rate in boreal autumn, with more than 30% below 700 hPa and

465   up to 50% near the surface (Figure 10c). It is related to the prevalence of HLD and relatively

466   cold temperatures during this time in the Arctic. This is not the case for the summer, when the

467   freezing level is relatively high. Although it is responsible for 50% of the total Arctic dust

468   burden in the boreal summer, HLD has a limited contribution to the immersion freezing rate in

469   the clouds (Figure 10b), because its weak vertical transport makes it hard to reach the freezing

470   line. The contrast results in summer and autumn suggest that the immersion freezing rate in the

471   Arctic clouds is influenced by air temperature in addition to the aerosols. It also implies that the

472   surface INP measurements may not reflect the complete picture of INP effects and more aircraft

473   INP measurements are needed in the future. The seasonal variations of the immersion freezing

474   rate from NAf and EAs are weaker than that from HLD but are still subjected to the vertical

475   temperature change with season. The North African dust contributes more in spring and winter,

476   while the East Asian dust is more important in summer and autumn.

477   **3.4 Impact on cloud properties and radiative fluxes**

478   Dust INPs can freeze the supercooled liquid droplets, which impacts the cloud microphysical

479   and macrophysical properties and modulates the Earth's radiative balance. To examine such

480   impacts, we conduct three sensitivity experiments that turn off the heterogeneous ice nucleation

481   in the mixed-phase clouds by dust from Arctic local source, North Africa, and East Asia,

482   respectively (i.e., noArc, noNAf, and noEAs in Table 1). The impacts of dust INPs from each

483   source are determined by subtracting the respective sensitivity experiment from CTRL. Due to

484   the feedbacks in dust emission and wet scavenging caused by changing cloud properties, the dust

485   concentrations in the sensitivity experiments are not identical to CTRL, but the absolute

486   differences are mostly within 5% (Figure S5 in the Supplement).

487   The cloud liquid and ice changes caused by dust INPs from each source are shown in Figure

488   11. Due to the strengthening of heterogeneous ice nucleation processes, INPs from all the three

489   sources consistently reduce the total liquid mass mixing ratio (TLIQ) (Figure 11, first column)

490   and cloud liquid droplet number concentration (NUMLIQ) (Figure 11, third column). The

491   influence of HLD is mainly in the lower troposphere (Fig. 11, top row) and the influence of LLD

492   extends to higher altitudes (Fig. 11, bottom two rows). Moreover, the cloud ice number

493   concentration (NUMICE) decreases in the upper troposphere (Figure 11, fourth column), likely

494   due to less cloud droplets available for the homogeneous freezing in cirrus cloud after

495   introducing dust INPs in the mixed-phase clouds. With fewer ice crystals falling from the cirrus

496   clouds to the mixed-phase clouds, the WBF process in the mixed-phase clouds is inhibited

497   (Figure S6). Other ice phase processes such as the accretion of cloud water by snow and the

498   growth of ice crystals by vapor deposition also become less efficient, which decreases the total

499   ice mass mixing ratio (TICE) above 600-700 hPa altitude (Figure 11, second column). TICE in

500   the lower troposphere is increased because of immersion freezing and snow sedimentation from

501   above.

502   Since liquid water path (LWP) is found to play a critical role in the Arctic radiative budget

503   (e.g., Dong et al., 2010; Hofer et al., 2019; Shupe and Intrieri, 2004), we further investigate the

504   seasonal variations of LWP changes caused by dust INPs from the three sources (Figure 12).

505   Corroborated with their large contribution to the immersion freezing rate during this time (Figure

506   10, top row), HLD INPs produce the strongest LWP decrease (-1.3 g m^{-2}) in boreal autumn

507   (Figure 12c), especially over North Canada and Greenland. The influence of LLD INPs on LWP

508   peaks in spring and winter. North African dust tends to have a larger impact on North Eurasia,

509   while East Asian dust impacts the west Arctic more.

510   Dust INPs from the three sources consistently increase (decrease) the annual mean

511   downwelling shortwave (longwave) radiative flux (FSDS and FLDS) at the surface (Figure 13,

512 left and middle columns). This is mainly due to the LWP decrease, which reduces the cloud

513 albedo and longwave cloud emissivity. For HLD INPs, the FLDS reduction dominates over the

514 FSDS increase and causes a net cooling effect at the Arctic surface (-0.24 W m^{-2}) (Figure 13c).

515 In contrast, FSDS and FLDS changes related to the LLD INPs are comparable, which cancels

516 each other and yields a small net radiative effect (0.08 W m^{-2} for NAf and -0.06 W m^{-2} for EAs)

517 (Figure 13, bottom two rows). These differences in the net radiative effect are associated with

518 different seasonalities of HLD and LLD. The insolation in the Arctic is strong in spring and

519 summer but very limited in autumn and winter. Since the HLD INPs have much stronger

520 influence on LWP in autumn and winter than spring and summer (Figure 12), their contribution

521 to the FSDS warming is weak and the FLDS cooling in autumn and winter dominates the annual

522 mean effect (Table 4, part 1; also seen in Figure S7 to S9). LLD INPs are also important in

523 spring and summer, so their FSDS warming effect is comparable to, and compensates for, the

524 FLDS cooling effect.

525   We also examined the dust INP effect on cloud radiative forcing (CRF) at the top of the

526 atmosphere (TOA) (Table 4, part 2). Dust INPs from the three sources induce a small net cooling

527 (from -0.03 to -0.05 W m^{-2}) in the Arctic, with SW warming and LW cooling effects. The net

528 cooling persists throughout the year, except for the summertime when the sufficient insolation

529 results in a strong SW warming and, consequently, a net warming effect. Shi and Liu (2019) also

530 found LLD can induce a generally net cooling effect above 70°N (0.18 to -1.95 W m^{-2}), but in a

531 much higher magnitude than the sum of NAf and EAs dust INP effects (-0.15 W m^{-2} above 70°N,

532 not shown in Table 4), which implies the aerosol glaciation effect on mixed-phase clouds is

533 highly non-linear.

534   Finally, we evaluate the model performance in simulating the Arctic LWP and radiative fluxes

535   against the Moderate Resolution Imaging Spectroradiometer (MODIS) LWP (Platnick et al.,

536   2003) and the Cloud and the Earth's Radiant Energy System Energy Balanced and Filled Edition

537   4.1 (CERES-EBAF Ed4.1) products (Loeb et al., 2018; Kato et al., 2018), respectively (Figure

538   14). Two MODIS datasets are used, including the standard product (Platnick et al., 2003; P03)

539   and an improved one (Khanal et al., 2020; K20) that corrected the positive bias in the Arctic in

540   P03. The MODIS simulator is used for the LWP comparison. According to Fig. 14, the simulated

541   LWP from the four experiments are lower than P03 but higher than K20. All the four

542   experiments also underestimate FSDS with too strong SWCF and overestimate FLDS with too

543   strong LWCF, which likely points to the biases of modeled clouds (e.g., too much LWP as

544   compared to K20). The differences among the model experiments are very small compared to

545   their discrepancies with observations. We notice including dust INPs from the three sources

546   decreases the simulated LWP (i.e., CTRL has less LWP than the other experiments) (Figure 14a),

547   which makes the model performance better if compared to K20. Moreover, it shows noticeable

548   improvements in simulating both surface and TOA radiative fluxes after including dust INPs

549   from each of the three sources (i.e., the results from CTRL are closer to the CERES results than

550   the other three experiments) (Figure 14b-e).

551   Overall, including HLD or LLD INPs do not contribute a lot to the reduction of biases in

552   simulating the LWP and radiative fluxes in the AMPCs. However, the representation of AMPCs

553   in global climate models is associated with multiple cloud macro- and microphysical processes,

554   and large-scale dynamics (Morrison et al., 2012) (see more discussion in Section 4), which

555   interact with one another non-linearly. Therefore, even though including HLD or LLD INPs do

556   not improve the representation of AMPCs significantly in our model, a good representation of

557   dust INPs, especially including HLD INPs, could still be of great importance for parameterizing

558   AMPCs in the model.

559   **4. Discussion**

560   The HLD emission in our CTRL simulation is manually tuned up by 10 times to match the

561   estimate by Bullard et al. (2016), which is derived by compiling field measurements in Iceland

562   and Alaska. Since the instruments were operated under extreme Arctic conditions and the

563   sampling is very scarce, this estimate may have large uncertainties. Therefore, the tuned HLD

564   emission can be biased as well. Considering the overestimation of Greenland dust deposition,

565   summertime surface dust concentrations at Alert station, and surface INP concentrations at

566   Svalbald, our tuning may cause a regional and temporal high bias in HLD dust emissions. We

567   examine this uncertainty by conducting a sensitivity experiment with halving HLD emissions in

568   CTRL (i.e., HLD_half) and analysing the interannual variability of CTRL and HLD_half

569   simulations (Table S2 and Figures S10-S11). The HLD_half simulation indeed has a better

570   performance than CTRL. However, the high bias for Greenland deposition and the summertime

571   overestimation of Alert dust surface concentration still exist, which reflects the limitation of the

572   dust emission parameterization we use. This parameterization may not be able to capture the

573   spatial distribution of dust emissions across the Arctic, considering that the model performance

574   at other sites (e.g., Heimaey, Figure 3a) is much better. Also, the HLD emissions and their

575   regional distributions have large interannual variabilities. Therefore, as we mentioned in Section

576   3.1, comparing model simulations with measurements conducted in different years may result in

577   large uncertainties.

578   The overestimation of surface dust and INP concentrations may imply a too weak vertical

579   transport of HLD, considering the low biases of dust in the upper troposphere as compared with

580   ARCTAS measurements and CALIPSO retrievals. The weak vertical transport at the source

581   regions in EAMv1 was also found in Wu et al. (2020), which was related to the too strong dry

582   deposition at the surface layer. If this bias is addressed, HLD would contribute less (more) to the

583   Arctic dust concentrations in the lower (upper) troposphere, which suggests a larger contribution

584   of HLD to the heterogeneous ice nucleation in the mixed-phase clouds in the summertime. As a

585   result, the HLD would induce a more positive net downwelling radiative flux at the surface in

586   summer and a less negative annual mean radiative effect. It is also noted that the underprediction

587   in the upper troposphere dust may come from a weak long-range transport of LLD. If this is the

588   case, the HLD would have a weaker contribution to the upper level dust concentrations and

589   likely less of an impact on mixed-phase cloud heterogeneous ice nucleation in the summertime.

590   In addition, EAMv1 has intrinsic biases in its cloud microphysics parameterizations. As

591   mentioned in Section 2.1, the WBF process rate in EAMv1 is tuned down by a factor of 10,

592   which results in too many supercooled liquid clouds in high latitudes (Y. Zhang et al., 2019; M.

593   Zhang et al., 2020). Shi and Liu (2019) found the sign and magnitude of dust INP cloud radiative

594   effect in the Arctic would change, after removing the tuning factor for the WBF process in

595   EAMv1. Moreover, EAMv1 does not account for several secondary ice production mechanisms,

596   which are suggested to have a large impact on the ice crystal number concentrations and thus

597   cloud phase (Zhao and Liu, 2021; Zhao et al., 2021b). All these uncertainties in the cloud

598   microphysical processes would interact non-linearly and influence our estimate of INP radiative

599   effect and should be addressed in future studies.

5. Conclusions

In this study, we investigate the source attribution of dust aerosols in the Arctic and quantify the relative importance of Arctic local dust versus long-range transported LLD to the Arctic dust loading and INP population. We found that HLD is responsible for 30.7% of the total dust burden in the Arctic, whereas LLD from Asia and North Africa contributes 44.2% and 24.2%, respectively. The vertical transport of HLD is limited due to the stable cold air in the Arctic and thus it contributes more to the dust burden in the lower troposphere. In boreal summer and autumn when the contribution of HLD is at a maximum because of stronger local dust emissions, HLD is responsible for more than 30% of the Arctic dust loading below 800 hPa, but less than 10% above 700 hPa. In contrast, LLD from North African and East Asian dust dominates the dust burden in the free troposphere, since the poleward transport of LLD follows the uplifted isentropes. The North African and East Asian dust accounts for about two thirds of the dust loading above 700 hPa, with the remaining one third from other LLD sources. The North African dust contributes more between 500 and 700 hPa, while the East Asian dust dominates in the upper troposphere (above 400 hPa) because of its high emission heights. In addition, the North Africa source has a larger contribution in springtime, while the other three seasons are more influenced by the East Asian source.

Modeled dust INP concentrations are investigated following two ice nucleation parameterizations: D15 and SM20. Compared with INP measurements, our results show that including HLD as INPs significantly improves the model performance in simulating Arctic INP concentrations, especially for the ground measurements and for the measurements conducted in summer and autumn. We also examine the INP contributions from BC and SSA based on Sc20 and M18, respectively. The model suggests that both of them are only weak sources compared

28

623   with dust. We note that the model may underestimate SSA INPs and currently misses the

624   representation of terrestrial biological INPs. The model biases of INPs can also be due to bias in

625   simulating Arctic dust concentrations and/or the uncertainties in ice nucleation parameterizations.

626   We examine the contribution of dust from the three sources (Arctic, North Africa, and East

627   Asia) to the ambient immersion freezing rate in the Arctic. The contribution from HLD shows a

628   strong seasonal variation, with the peak contribution in boreal autumn (above 20% below 500

629   hPa). In summer, although HLD has strong contributions to the dust loading and INP

630   concentrations in the lower troposphere, its impact on the ambient immersion freezing rate is

631   limited due to the warm temperatures and weak vertical transport. This finding implies that

632   surface INP measurements may not be sufficient in representing the INP population in the Arctic

633   mixed-phase clouds and more measurements of INP vertical profiles are needed in the future.

634   North African and East Asian dust are the two major LLD contributors to the ambient immersion

635   freezing rate. The annual mean contribution (30-40%) from North African dust peaks at around

636   500 hPa, while the immersion freezing is dominated by East Asian dust (more than 40%) in the

637   upper troposphere (above 400 hPa).

638   The cloud glaciation effect of dust INPs from local Arctic sources, and North African and East

639   Asian sources, is further examined. It is found that INPs from all the three sources consistently

640   result in a reduction in TLIQ and NUMLIQ. TICE and NUMICE at higher altitude also decrease,

641   likely due to the weakening of homogeneous freezing in cirrus clouds. LWP reduction caused by

642   HLD INPs is evident in autumn and winter, while those by dust INPs from the two LLD sources

643   peak in spring. HLD INPs also drive a net cooling effect of -0.24 W m^{-2} in the downwelling

644   radiative flux at the surface in the Arctic, while the net radiative effects of the two LLD INP

645   sources are relatively small (0.08 W m^{-2} for NAf and -0.06 W m^{-2} for EAs). This variation in

646 radiative effect reflects the seasonal difference between HLD and LLD. Our results also suggest

647 that all the three dust sources result in a weak negative net cloud radiative effect (-0.03 to -0.05

648 W m^{-2}) in the Arctic, which is consistent with Shi and Liu (2019).

649   Overall, our study shows that the Arctic local dust, which has been overlooked in previous

650 studies, may have large contributions to the Arctic dust loading and INP population. It can also

651 influence the Arctic mixed-phase cloud properties by acting as INPs. Considering the climate

652 impacts of local Arctic dust emissions will be important given a warming climate, where

653 reduction in snow coverage and more exposure of dryland in the Arctic may lead to increased

654 HLD emissions.

655 *Code availability.* The E3SM code is available on GitHub: https://github.com/E3SM-

656 Project/E3SM.git.

657 *Author contribution.* YS and XL conceived the project. YS modified the code, conducted the

658 simulations, and led the analyses with suggestions from XL, MW, XZ, ZK, and HB. XL

659 supervised the study. YS wrote the first draft of the paper. All coauthors were involved in helpful

660 discussions and revised the paper.

661 *Competing interests.* The authors declare that they have no conflict of interest.

References

674 Albani, S., Mahowald, N. M., Perry, A. T., Scanza, R. A., Zender, C. S., Heavens, N. G., Maggi,
675 V., Kok, J. F., and Otto-Bliesner, B. L.: Improved dust representation in the Community
676 Atmosphere Model, J. Adv. Model. Earth Syst., 6, 541–570,
677 https://doi.org/10.1002/2013MS000279, 2014.

678 Arimoto, R., Duce, R. A., Ray, B. J., Ellis Jr, W. G., Cullen, J. D., and Merrill, J. T.: Trace
679 elements in the atmosphere over the North Atlantic, J. Geophys. Res. Atmos., 100(D1), 1199–
680 1213, https://doi.org/10.1029/94JD02618, 1995.

681 Arnalds, O., Dagsson-Waldhauserova, P., and Olafsson, H.: The Icelandic volcanic aeolian
682 environment: Processes and impacts — A review, Aeolian Res., 20, 176–195,
683 https://doi.org/10.1016/j.aeolia.2016.01.004, 2016.

684 Atkinson, J. D., Murray, B. J., Woodhouse, M. T., Whale, T. F., Baustian, K. J., Carslaw, K. S.,
685 Dobbie, S., O'Sullivan, D., and Malkin, T. L.: The importance of feldspar for ice nucleation by
686 mineral dust in mixed-phase clouds, Nature, 498, 355–358, https://doi.org/10.1038/nature12278,
687 2013.

688 Baddock, M. C., Mockford, T., Bullard, J. E., and Thorsteinsson, T.: Pathways of high-latitude
689 dust in the North Atlantic, Earth Planet. Sci. Lett., 459, 170–182,
690 https://doi.org/10.1016/j.epsl.2016.11.034, 2017.

691 de Boer, G., Morrison, H., Shupe, M. D., and Hildner, R.: Evidence of liquid dependent ice
692 nucleation in high-latitude stratiform clouds from surface remote sensors, Geophys. Res. Lett.,
693 38, L01803, https://doi.org/10.1029/2010GL046016, 2011.

694 Bogenschutz, P. A., Gettelman, A., Morrison, H., Larson, V. E., Craig, C., and Schanen, D. P.:
695 Higher-order turbulence closure and its impact on climate simulations in the community
696 atmosphere model, J. Clim., 26, 9655–9676, https://doi.org/10.1175/JCLI-D-13-00075.1, 2013.

697   Bory, A. J.-M., Biscaye, P. E., Svensson, A., and Grousset, F. E.: Seasonal variability in the
698   origin of recent atmospheric mineral dust at NorthGRIP, Greenland, Earth Planet. Sci. Lett., 196,
699   123–134, https://doi.org/10.1016/S0012-821X(01)00609-4, 2002.

700   Bory, A. J.-M., Biscaye, P. E., and Grousset, F. E.: Two distinct seasonal Asian source regions
701   for mineral dust deposited in Greenland (NorthGRIP), Geophys. Res. Lett., 30,
702   https://doi.org/10.1029/2002GL016446, 2003.

703   Breider, T. J., Mickley, L. J., Jacob, D. J., Wang, Q., Fisher, J. A., Chang, R. Y.-W., and
704   Alexander, B.: Annual distributions and sources of Arctic aerosol components, aerosol optical
705   depth, and aerosol absorption, J. Geophys. Res. Atmos., 119, 4107–4124,
706   https://doi.org/10.1002/2013JD020996, 2014.

707   Bullard, J. E.: The distribution and biogeochemical importance of high-latitude dust in the Arctic
708   and Southern Ocean-Antarctic regions, J. Geophys. Res. Atmos., 122, 3098–3103,
709   https://doi.org/10.1002/2016JD026363, 2017.

710   Bullard, J. E. and Austin, M. J.: Dust generation on a proglacial floodplain, West Greenland,
711   Aeolian Res., 3, 43–54, https://doi.org/10.1016/j.aeolia.2011.01.002, 2011.

712   Bullard, J. E., Baddock, M., Bradwell, T., Crusius, J., Darlington, E., Gaiero, D., Gassó, S.,
713   Gisladottir, G., Hodgkins, R., McCulloch, R., McKenna-Neuman, C., Mockford, T., Stewart, H.,
714   and Thorsteinsson, T.: High-latitude dust in the Earth system, Rev. Geophys., 54, 447–485,
715   https://doi.org/10.1002/2016RG000518, 2016.

716   Creamean, J. M., Kirpes, R. M., Pratt, K. A., Spada, N. J., Maahn, M., de Boer, G., Schnell, R.
717   C., and China, S.: Marine and terrestrial influences on ice nucleating particles during continuous
718   springtime measurements in an Arctic oilfield location, Atmos. Chem. Phys., 18, 18023–18042,
719   https://doi.org/10.5194/acp-18-18023-2018, 2018.

720   Creamean, J. M., Hill, T. C. J., DeMott, P. J., Uetake, J., Kreidenweis, S., and Douglas, T. A.:
721   Thawing permafrost: an overlooked source of seeds for Arctic cloud formation, Environ. Res.
722   Lett., 15, 084022, https://doi.org/10.1088/1748-9326/ab87d3, 2020.

723   Crusius, J., Schroth, A. W., Gassó, S., Moy, C. M., Levy, R. C., and Gatica, M.: Glacial flour
724   dust storms in the Gulf of Alaska: Hydrologic and meteorological controls and their importance
725   as a source of bioavailable iron, Geophys. Res. Lett., 38, L06602,
726   https://doi.org/10.1029/2010GL046573, 2011.

727   Dagsson-Waldhauserova, P., Arnalds, O., and Olafsson, H.: Long-term variability of dust events
728   in Iceland (1949–2011), Atmos. Chem. Phys., 14, 13411–13422, https://doi.org/10.5194/acp-14-
729   13411-2014, 2014.

730   DeMott, P. J., Sassen, K., Poellot, M. R., Baumgardner, D., Rogers, D. C., Brooks, S. D., Prenni,
731   A. J., and Kreidenweis, S. M.: African dust aerosols as atmospheric ice nuclei, Geophys. Res.
732   Lett., 30(14), 1732, https://doi.org/10.1029/2003GL017410, 2003.

733 DeMott, P. J., Prenni, A. J., Liu, X., Kreidenweis, S. M., Petters, M. D., Twohy, C. H.,
734 Richardson, M. S., Eidhammer, T., and Rogers, D. C.: Predicting global atmospheric ice nuclei
735 distributions and their impacts on climate, Proc. Natl. Acad. Sci. U.S.A., 107(25), 11217–11222,
736 https://doi.org/10.1073/pnas.0910818107, 2010.

737 DeMott, P. J., Prenni, A. J., McMeeking, G. R., Sullivan, R. C., Petters, M. D., Tobo, Y.,
738 Niemand, M., Möhler, O., Snider, J. R., Wang, Z., and Kreidenweis, S. M.: Integrating
739 laboratory and field data to quantify the immersion freezing ice nucleation activity of mineral
740 dust particles, Atmos. Chem. Phys., 15, 393–409, https://doi.org/10.5194/acp-15-393-2015, 2015.

741 Dong, X., Xi, B., Crosby, K., Long, C. N., Stone, R. S., and Shupe, M. D.: A 10 year
742 climatology of Arctic cloud fraction and radiative forcing at Barrow, Alaska, J. Geophys. Res.
743 Atmos., 115, D17212, https://doi.org/10.1029/2009JD013489, 2010.

744 Dörnbrack, A., Stachlewska, I. S., Ritter, C., and Neuber, R.: Aerosol distribution around
745 Svalbard during intense easterly winds, Atmos. Chem. Phys., 10, 1473–1490,
746 https://doi.org/10.5194/acp-10-1473-2010, 2010.

747 Fenn, R. W. and Weickmann, H. K.: Some results of aerosol measurements, Geofisica Pura e
748 Applicata, 42, 53–61, https://doi.org/10.1007/BF02113389, 1959.

749 Gettelman, A. and Morrison, H.: Advanced two-moment bulk microphysics for global models.
750 Part I: off-line tests and comparison with other schemes, J. Clim., 28, 1268–1287,
751 https://doi.org/10.1175/JCLI-D-14-00102.1, 2015.

752 Ghan, S. J. and Zaveri, R. A.: Parameterization of optical properties for hydrated internally
753 mixed aerosol, J. Geophys. Res., 112, D10201, https://doi.org/10.1029/2006JD007927, 2007.

754 Ginoux, P., Chin, M., Tegen, I., Prospero, J. M., Holben, B., Dubovik, O., and Lin, S.-J.: Sources
755 and distributions of dust aerosols simulated with the GOCART model, J. Geophys. Res., 106,
756 20255–20273, https://doi.org/10.1029/2000JD000053, 2001.

757 Golaz, J.-C., Larson, V. E., and Cotton, W. R.: A PDF-based model for boundary layer clouds.
758 Part I: Method and model description, J. Atmos. Sci., 59, 3540-3551,
759 https://doi.org/10.1175/1520-0469(2002)059<3540:APBMFB>2.0.CO;2, 2002.

760 Groot Zwaaftink, C. D., Grythe, H., Skov, H., and Stohl, A.: Substantial contribution of northern
761 high-latitude sources to mineral dust in the Arctic, J. Geophys. Res. Atmos., 121, 13678-13697,
762 https://doi.org/10.1002/2016JD025482, 2016.

763 Hiranuma, N., Brooks, S. D., Moffet, R. C., Glen, A., Laskin, A., Gilles, M. K.m Liu, P.,
764 Macdonald, A. M., Strapp, J. W., McFarquhar, G. M: Chemical characterization of individual
765 particles and residuals of cloud droplets and ice crystals collected on board research aircraft in
766 the ISDAC 2008 study, J. Geophys. Res. Atmos., 118, 6564-6579,
767 https://doi.org/10.1002/jgrd.50484, 2013.

768 Hofer, S., Tedstone, A. J., Fettweis, X., and Bamber, J. L.: Cloud microphysics and circulation
769 anomalies control differences in future Greenland melt, Nat. Clim. Chang., 9, 523–528,
770 https://doi.org/10.1038/s41558-019-0507-8, 2019.

771 Holben, B. N., Eck, T. F., Slutsker, I., Tanré, D., Buis, J. P., Setzer, A., Vermote, E., Reagan, J.
772 A., Kaufman, Y. J., Nakajima, T., Lavenu, F., Jankowiak, I., and Smirnov, A.: AERONET—A
773 Federated Instrument Network and Data Archive for Aerosol Characterization, Remote Sens.
774 Environ., 66, 1–16, https://doi.org/10.1016/S0034-4257(98)00031-5, 1998.

775 Hoose, C. and Möhler, O.: Heterogeneous ice nucleation on atmospheric aerosols: a review of
776 results from laboratory experiments, Atmos. Chem. Phys., 12, 9817–9854,
777 https://doi.org/10.5194/acp-12-9817-2012, 2012.

778 Huang, Z., Huang, J., Hayasaka, T., Wang, S., Zhou, T., and Jin, H.: Short-cut transport path for
779 Asian dust directly to the Arctic: a case study, Environ. Res. Lett., 10, 114018,
780 https://doi.org/10.1088/1748-9326/10/11/114018, 2015.

781 Huneeus, N., Schulz, M., Balkanski, Y., Griesfeller, J., Prospero, J., Kinne, S., Bauer, S.,
782 Boucher, O., Chin, M., Dentener, F., Diehl, T., Easter, R., Fillmore, D., Ghan, S., Ginoux, P.,
783 Grini, A., Horowitz, L., Koch, D., Krol, M. C., Landing, W., Liu, X., Mahowald, N., Miller, R.,
784 Morcrette, J.-J., Myhre, G., Penner, J., Perlwitz, J., Stier, P., Takemura, T., and Zender, C. S.:
785 Global dust model intercomparison in AeroCom phase I, Atmos. Chem. Phys., 11, 7781–7816,
786 https://doi.org/10.5194/acp-11-7781-2011, 2011.

787 Irish, V. E., Hanna, S. J., Willis, M. D., China, S., Thomas, J. L., Wentzell, J. J. B., Cirisan, A.,
788 Si, M., Leaitch, W. R., Murphy, J. G., Abbatt, J. P. D., Laskin, A., Girard, E., and Bertram, A. K.:
789 Ice nucleating particles in the marine boundary layer in the Canadian Arctic during summer 2014,
790 Atmos. Chem. Phys., 19, 1027–1039, https://doi.org/10.5194/acp-19-1027-2019, 2019.

791 Jacob, D. J., Crawford, J. H., Maring, H., Clarke, A. D., Dibb, J. E., Emmons, L. K., Ferrare, R.
792 A., Hostetler, C. A., Russell, P. B., Singh, H. B., Thompson, A. M., Shaw, G. E., McCauley, E.,
793 Pederson, J. R., and Fisher, J. A.: The Arctic Research of the Composition of the Troposphere
794 from Aircraft and Satellites (ARCTAS) mission: design, execution, and first results, Atmos.
795 Chem. Phys., 10, 5191–5212, https://doi.org/10.5194/acp-10-5191-2010, 2010.

796 Kato, S., Rose, F. G., Rutan, D. A., Thorsen, T. E., Loeb, N. G., Doelling, D. R., Huang, X.,
797 Smith, W. L., Su, W., and Ham, S.-H.: Surface irradiances of Edition 4.0 Clouds and the Earth's
798 Radiant Energy System (CERES) Energy Balanced and Filled (EBAF) data product, J. Climate,
799 31, 4501-4527, https://doi.org/10.1175/JCLI-D-17-0523.1, 2018.

800 Khanal, S., Wang, Z., and French, J. R.: Improving middle and high latitude cloud liquid water
801 path measurements from MODIS, Atmos. Res., 243. 105033.
802 https://doi.org/10.1016/j.atmosres.2020.105033, 2020.

803 Kinne, S., Schulz, M., Textor, C., Guibert, S., Balkanski, Y., Bauer, S. E., Berntsen, T., Berglen,
804 T. F., Boucher, O., Chin, M., Collins, W., Dentener, F., Diehl, T., Easter, R., Feichter, J.,
805 Fillmore, D., Ghan, S., Ginoux, P., Gong, S., Grini, A., Hendricks, J., Herzog, M., Horowitz, L.,
806 Isaksen, I., Iversen, T., Kirkevåg, A., Kloster, S., Koch, D., Kristjansson, J. E., Krol, M., Lauer,

807 A., Lamarque, J. F., Lesins, G., Liu, X., Lohmann, U., Montanaro, V., Myhre, G., Penner, J.,
808 Pitari, G., Reddy, S., Seland, O., Stier, P., Takemura, T., and Tie, X.: An AeroCom initial
809 assessment – optical properties in aerosol component modules of global models, Atmos. Chem.
810 Phys., 6, 1815–1834, https://doi.org/10.5194/acp-6-1815-2006, 2006.

811 Kohfeld, K. E. and Harrison, S. P.: DIRTMAP: the geological record of dust, Earth-Sci. Rev., 54,
812 81–114, https://doi.org/10.1016/S0012-8252(01)00042-3, 2001.

813 Kok, J. F.: A scaling theory for the size distribution of emitted dust aerosols suggests climate
814 models underestimate the size of the global dust cycle, Proc. Natl. Acad. Sci. U.S.A., 108(3),
815 1016–1021, https://doi.org/10.1073/pnas.1014798108, 2011.

816 Kok, J. F., Mahowald, N. M., Fratini, G., Gillies, J. A., Ishizuka, M., Leys, J. F., Mikami, M.,
817 Park, M.-S., Park, S.-U., Van Pelt, R. S., and Zobeck, T. M.: An improved dust emission model –
818 Part 1: Model description and comparison against measurements, Atmos. Chem. Phys., 14,
819 13023–13041, https://doi.org/10.5194/acp-14-13023-2014, 2014a.

820 Kok, J. F., Albani, S., Mahowald, N. M., and Ward, D. S.: An improved dust emission model –
821 Part 2: Evaluation in the Community Earth System Model, with implications for the use of dust
822 source functions, Atmos. Chem. Phys., 14, 13043–13061, https://doi.org/10.5194/acp-14-13043-
823 2014, 2014b.

824 Kok, J. F., Ridley, D. A., Zhou, Q., Miller, R. L., Zhao, C., Heald, C. L., Ward, D. S., Albani, S.,
825 and Haustein, K.: Smaller desert dust cooling effect estimated from analysis of dust size and
826 abundance, Nat. Geosci., 10, 274–278, https://doi.org/10.1038/ngeo2912, 2017.

827 Larson, V. E., Golaz, J.-C., and Cotton, W. R.: Small-Scale and Mesoscale Variability in Cloudy
828 Boundary Layers: Joint Probability Density Functions, J. Atmos. Sci., 59, 3519-3539,
829 https://doi.org/10.1175/1520-0469(2002)059<3519:SSAMVI>2.0.CO;2, 2002.

830 Liu, X., Xie, S., Boyle, J., Klein, S. A., Shi, X., Wang, Z., Lin, W., Ghan, S. J., Earle, M., Liu, P.
831 S. K., and Zelenyuk, A.: Testing cloud microphysics parameterizations in NCAR CAM5 with
832 ISDAC   and   M-PACE   observations,   J.   Geophys.   Res.,   116,   D00T11,
833 https://doi.org/10.1029/2011JD015889, 2011.

834 Liu, X., Ma, P.-L., Wang, H., Tilmes, S., Singh, B., Easter, R. C., Ghan, S. J., and Rasch, P. J.:
835 Description and evaluation of a new four-mode version of the Modal Aerosol Module (MAM4)
836 within version 5.3 of the Community Atmosphere Model, Geosci. Model Dev., 9, 505–522,
837 https://doi.org/10.5194/gmd-9-505-2016, 2016.

838 Loeb, N. G., Doelling, D. R., Wang, H., Su, W., Nguyen, C., Corbett, J. G., Liang, L., Mitrescu,
839 C., Rose, F. G., and Kato, S.: Clouds and the Earth's Radiant Energy System (CERES) Energy
840 Balanced and Filled (EBAF) Top-of-Atmosphere (TOA) Edition-4.0 Data Product. J. Climate,
841 31, 895-918, https://doi.org/ 10.1175/JCLI-D-17-0208.1, 2018.

842 Luo, C., Mahowald, N. M., and Corral, J. del: Sensitivity study of meteorological parameters on
843 mineral aerosol mobilization, transport, and distribution, J. Geophys. Res., 108, 4447,
844 https://doi.org/10.1029/2003JD003483, 2003.

Luo, T., Wang, Z., Ferrare, R. A., Hostetler, C. A., Yuan, R., and Zhang, D.: Vertically resolved separation of dust and other aerosol types by a new lidar depolarization method, Opt. Express, 23, 14095-14107, https://doi.org/10.1364/OE.23.014095, 2015a.

Luo, T., Wang, Z., Zhang, D., Liu, X., Wang, Y., and Yuan, R.: Global dust distribution from improved thin dust layer detection using A-train satellite lidar observations, Geophys. Res. Lett., 42, 620–628, https://doi.org/10.1002/2014GL062111, 2015b.

Maenhaut, W., Fernandez-Jimenez, M.-T., Rajta, I., Dubtsov, S., Meixner, F. X., Andreae, M. O., Torr, S., Hargrove, J. W., Chimanga, P., and Mlambo, J.: Long-term aerosol composi- tion measruments and source apportionment at Rukomechi, Zim- babwe, J. Aerosol Sci., 31(Suppl. 1), S469–S470, 2000a.

Maenhaut, W., Fernandez-Jimenez, M.-T., Vanderzalm, J. L., Hooper, B. M., Hooper, M. A., and Tapper, N. J.: Aerosol com- position at Jabiru, Australia and impact of biomass burning, J. Aerosol Sci., 31(Suppl. 1), S745–S746, 2000b.

Mahowald, N. M., Engelstaedter, S., Luo, C., Sealy, A., Artaxo, P., Benitez-Nelson, C., Bonnet, S., Chen, Y., Chuang, P. Y., Cohen, D. D., Dulac, F., Herut, B., Johansen, A. M., Kubilay, N., Losno, R., Maenhaut, W., Paytan, A., Prospero, J. M., Shank, L. M., and Siefert, R. L.: Atmospheric iron deposition: global distribution, variability, and human perturbations, Ann. Rev. Mar. Sci., 1, 245–278, https://doi.org/10.1146/annurev.marine.010908.163727, 2009.

Mason, R. H., Si, M., Chou, C., Irish, V. E., Dickie, R., Elizondo, P., Wong, R., Brintnell, M., Elsasser, M., Lassar, W. M., Pierce, K. M., Leaitch, W. R., MacDonald, A. M., Platt, A., Toom-Sauntry, D., Sarda-Estève, R., Schiller, C. L., Suski, K. J., Hill, T. C. J., Abbatt, J. P. D., Huffman, J. A., DeMott, P. J., and Bertram, A. K.: Size-resolved measurements of ice-nucleating particles at six locations in North America and one in Europe, Atmos. Chem. Phys., 16, 1637–1651, https://doi.org/10.5194/acp-16-1637-2016, 2016.

McCluskey, C. S., Ovadnevaite, J., Rinaldi, M., Atkinson, J., Belosi, F., Ceburnis, D., Marullo, S., Hill, T. C. J., Lohmann, U., Kanji, Z. A., O'Dowd, C., Kreidenweis, S. M., and DeMott, P. J.: Marine and terrestrial organic ice-nucleating particles in pristine marine to continentally influenced Northeast Atlantic air masses, J. Geophys. Res. Atmos., 123, 6196–6212, https://doi.org/10.1029/2017JD028033, 2018.

McFarquhar, G. M., Ghan, S., Verlinde, J., Korolev, A., Strapp, J. W., Schmid, B., Tomlinson, J. M., Wolde, M., Brooks, S. D., Cziczo, D., Dubey, M. K., Fan, J., Flynn, C., Gultepe, I., Hubbe, J., Gilles, M. K., Laskin, A., Lawson, P., Leaitch, W. R., Liu, P., Liu, X., Lubin, D., Mazzoleni, C., Macdonald, A.-M., Moffet, R. C., Morrison, H., Ovchinnikov, M., Shupe, M. D., Turner, D. D., Xie, S., Zelenyuk, A., Bae, K., Freer, M., and Glen, A.: Indirect and Semi-direct Aerosol Campaign: The Impact of Arctic Aerosols on Clouds, Bull. Amer. Meteor. Soc., 92, 183–201, https://doi.org/10.1175/2010BAMS2935.1, 2011.

Morrison, H., de Boer, G., Feingold, G., Harrington, J., Shupe, M. D., and Sulia, K.: Resilience of persistent Arctic mixed-phase clouds, Nat. Geosci., 5, 11–17, https://doi.org/10.1038/ngeo1332, 2012.

Murray, B. J., O'Sullivan, D., Atkinson, J. D., and Webb, M. E.: Ice nucleation by particles immersed in supercooled cloud droplets, Chem. Soc. Rev., 41, 6519-6554, https://doi.org/10.1039/c2cs35200a, 2012.

Paramonov, M., David, R. O., Kretzschmar, R., and Kanji, Z. A.: A laboratory investigation of the ice nucleation efficiency of three types of mineral and soil dust, Atmos. Chem. Phys., 18, 16515–16536, https://doi.org/10.5194/acp-18-16515-2018, 2018.

Platnick, S., King, M. D., Ackerman, S. A., Menzel, W. P., Baum, B. A., Riédi, J. C., & Frey, R. A.: The MODIS cloud products: Algorithms and examples from terra, IEEE Trans. Geosci. Remote Sens., 41(2), 459-472. https://doi.org/10.1109/ TGRS.2002.808301

Prenni, A. J., Harrington, J. Y., Tjernström, M., DeMott, P. J., Avramov, A., Long, C. N., Kreidenweis, S. M., Olsson, P. Q., and Verlinde, J.: Can ice-nucleating aerosols affect Arctic seasonal climate?, Bull. Amer. Meteor. Soc., 88, 541–550, https://doi.org/10.1175/BAMS-88-4-541, 2007.

Prenni, A. J., Demott, P. J., Rogers, D. C., Kreidenweis, S. M., Mcfarquhar, G. M., Zhang, G., and Poellot, M. R.: Ice nuclei characteristics from M-PACE and their relation to ice formation in clouds, Tellus B, 61, 436–448, https://doi.org/10.1111/j.1600-0889.2009.00415.x, 2009.

Prospero, J. M.: The Atmospheric Transport of Particles to the Ocean, in: Particle Flux in the Ocean, edited by: Ittekkot, V., Sch¨afer, P., Honjo, S., and Depetris, P. J., John Wiley & Sons Ltd., New York, 1996.

Prospero, J. M., Bullard, J. E., and Hodgkins, R.: High-Latitude Dust Over the North Atlantic: Inputs from Icelandic Proglacial Dust Storms, Science, 335, 1078–1082, https://doi.org/10.1126/science.1217447, 2012.

Prospero, J. M., Uematsu, M., and Savoie, D. L.: Mineral aerosol transport to the Pacific Ocean, edited by: Riley, J. P., 187–218, Academic Press, New York, 1989.

Rasch, P. J., Xie, S., Ma, P. -L., Lin, W., Wang, H., Tang, Q., Burrows, S. M., Caldwell, P., Zhang, K., Easter, R. C., Cameron-Smith, P., Singh, B., Wan, H., Golaz, J. -C., Harrop, B. E., Roesler, E., Bacmeister, J., Larson, V. E., Evans, K. J., Qian, Y., Taylor, M., Leung, L. R., Zhang, Y., Brent, L., Branstetter, M., Hannay, C., Mahajan, S., Mametjanov, A., Neale, R., Richter, J. H., Yoon, J. -H., Zender, C. S., Bader, D., Flanner, M., Foucar, J. G., Jacob, R., Keen, N., Klein, S. A., Liu, X., Salinger, A. G., Shrivastava, M., and Yang, Y.: An overview of the atmospheric component of the Energy Exascale Earth System Model, J. Adv. Model. Earth Syst., 11, 2377–2411, https://doi.org/10.1029/2019MS001629, 2019.

Ridley, D. A., Heald, C. L., Kok, J. F., and Zhao, C.: An observationally constrained estimate of global dust aerosol optical depth, Atmos. Chem. Phys., 16, 15097–15117, https://doi.org/10.5194/acp-16-15097-2016, 2016.

Sanchez-Marroquin, A., Arnalds, O., Baustian-Dorsi, K. J., Browse, J., Dagsson-Waldhauserova, P., Harrison, A. D., Maters, E. C., Pringle, K. J., Vergara-Temprado, J., Burke, I. T., McQuaid, J. B., Carslaw, K. S., and Murray, B. J.: Iceland is an episodic source of atmospheric ice-nucleating

922 particles relevant for mixed-phase clouds, Sci. Adv., 6, eaba8137,
923 https://doi.org/10.1126/sciadv.aba8137, 2020.

924 Schill, G. P., DeMott, P. J., Emerson, E. W., Rauker, A. M. C., Kodros, J. K., Suski, K. J., Hill, T.
925 C. J., Levin, E. J. T., Pierce, J. R., Farmer, D. K., and Kreidenweis, S. M.: The contribution of
926 black carbon to global ice nucleating particle concentrations relevant to mixed-phase clouds,
927 Proc. Natl. Acad. Sci. U.S.A., 117, 22705–22711, https://doi.org/10.1073/pnas.2001674117,
928 2020.

929 Schweiger, A. J., Lindsay, R. W., Vavrus, S., and Francis, J. A.: Relationships between Arctic
930 sea ice and clouds dusting autumn, J. Clim., 21, 4799-4810,
931 https://doi.org/10.1175/2008JCLI2156.1

932 Shao, Y., Wyrwoll, K.-H., Chappell, A., Huang, J., Lin, Z., McTainsh, G. H., Mikami, M.,
933 Tanaka, T. Y., Wang, X., and Yoon, S.: Dust cycle: An emerging core theme in Earth system
934 science, Aeolian Res., 2, 181–204, https://doi.org/10.1016/j.aeolia.2011.02.001, 2011.

935 Shi, Y. and Liu, X.: Dust Radiative Effects on Climate by Glaciating Mixed-Phase Clouds,
936 Geophys. Res. Lett., 46, 6128–6137, https://doi.org/10.1029/2019GL082504, 2019.

937 Shupe, M. D. and Intrieri, J. M.: Cloud Radiative Forcing of the Arctic Surface: The Influence of
938 Cloud Properties, Surface Albedo, and Solar Zenith Angle, J. Clim., 17, 616–628,
939 https://doi.org/10.1175/1520-0442(2004)017<0616:CRFOTA>2.0.CO;2, 2004.

940 Si, M., Evoy, E., Yun, J., Xi, Y., Hanna, S. J., Chivulescu, A., Rawlings, K., Veber, D., Platt, A.,
941 Kunkel, D., Hoor, P., Sharma, S., Leaitch, W. R., and Bertram, A. K.: Concentrations,
942 composition, and sources of ice-nucleating particles in the Canadian High Arctic during spring
943 2016, Atmos. Chem. Phys., 19, 3007–3024, https://doi.org/10.5194/acp-19-3007-2019, 2019.

944 Sirois, A., and Barrie, L. A.: Arctic lower tropospheric aerosol trends and composition at Alert,
945 Canada: 1980-1995, J. Geophys. Res. Atmos., 104, 11599-11618,
946 https://doi.org/10.1029/1999JD900077, 1999.

947 Smirnov, A., Holben, B. N., Eck, T. F., Dubovik, O., and Slutsker, I.: Cloud screening and
948 quality control algorithms for the AERONET database, Remote Sens. Environ., 73, 337–349,
949 https://doi.org/10.1016/S0034-4257(00)00109-7, 2000.

950 Stohl, A.: Characteristics of atmospheric transport into the Arctic troposphere, J. Geophys. Res.,
951 111, D11306, https://doi.org/10.1029/2005JD006888, 2006.

952 Stone, R., Anderson, G., Andrews, E., Dutton, E., Harris, J., Shettle, E., Berk, A.: Asian dust
953 signatures at Barrow: observed and simulated. Incursions and impact of Asian dust over
954 Northern Alaska, Workshop on Remote Sensing of Atmospheric Aerosols, IEEE Workshop on
955 Remote Sensing of Atmospheric Aerosols, 74-79,
956 https://doi.org/10.1109/AERSOL.2005.1494152, 2005.

957 Tan, I. and Storelvmo, T.: Sensitivity study on the influence of cloud microphysical parameters
958 on mixed-phase cloud thermodynamic phase partitioning in CAM5, J. Atmos. Sci., 73, 709-728,
959 https://doi.org/10.1175/JAS-D-15-0152.1, 2016.

960 Tan, I. and Storelvmo, T.: Evidence of Strong Contributions from Mixed-Phase Clouds to Arctic
961 Climate Change, Geophys. Res. Lett., 46, 2894–2902, https://doi.org/10.1029/2018GL081871,
962 2019.

963 Tanaka, T. Y. and Chiba, M.: A numerical study of the contributions of dust source regions to
964 the   global   dust   budget,   Glob.   Planet.   Change,   52,   88–104,
965 https://doi.org/10.1016/j.gloplacha.2006.02.002, 2006.

966 Tegen, I., Harrison, S. P., Kohfeld, K., Prentice, I. C., Coe, M., and Heimann, M.: Impact of
967 vegetation and preferential source areas on global dust aerosol: Results from a model study, J.
968 Geophys. Res. Atmos., 107, AAC 14-1-AAC 14-27, https://doi.org/10.1029/2001JD000963,
969 2002.

970 Tobo, Y., Adachi, K., DeMott, P. J., Hill, T. C. J., Hamilton, D. S., Mahowald, N. M., Nagatsuka,
971 N., Ohata, S., Uetake, J., Kondo, Y., and Koike, M.: Glacially sourced dust as a potentially
972 significant   source   of   ice   nucleating   particles,   Nat.   Geosci.,   12,   253–258,
973 https://doi.org/10.1038/s41561-019-0314-x, 2019.

974 Vali, G.: Nucleation terminology, Bull. Am. Meteorol. Soc., 66, 1426–1427, 1985.

975 Vali, G., DeMott, P. J., Möhler, O., and Whale, T. F.: Technical Note: A proposal for ice
976 nucleation terminology, Atmos. Chem. Phys., 15, 10263–10270, https://doi.org/10.5194/acp-15-
977 10263-2015, 2015.

978 VanCuren, R. A., Cahill, T., Burkhart, J., Barnes, D., Zhao, Y., Perry, K., Cliff, S., and
979 McConnell, J.: Aerosols and their sources at Summit Greenland – First results of continuous
980 size-   and   time-resolved   sampling,   Atmos.   Environ.,   52,   82–97,
981 https://doi.org/10.1016/j.atmosenv.2011.10.047, 2012.

982 Wang, H., Rasch, P. J., Easter, R. C., Singh, B., Zhang, R., Ma, P.-L., Qian, Y., Ghan, S. J., and
983 Beagley, N.: Using an explicit emission tagging method in global modeling of source-receptor
984 relationships for black carbon in the Arctic: Variations, sources, and transport pathways, J.
985 Geophys. Res. Atmos., 119, 12888-12909, https://doi.org/10.1002/2014JD022297, 2014.

986 Wang, H., Easter, R. C., Zhang, R., Ma, P.-L., Singh, B., Zhang, K., Ganguly, D., Rasch, P. J.,
987 Burrows, S. M., Ghan, S. J., Lou, S., Qian, Y., Yang, Y., Feng, Y., Flanner, M., Leung, L. R.,
988 Liu, X., Shrivastava, M., Sun, J., Tang, Q., Xie, S., and Yoon, J.: Aerosols in the E3SM Version
989 1: New Developments and Their Impacts on Radiative Forcing, J. Adv. Model. Earth Syst., 12,
990 e2019MS001851, https://doi.org/10.1029/2019MS001851, 2020.

991 Wang, Y., Liu, X., Hoose, C., and Wang, B.: Different contact angle distributions for
992 heterogeneous ice nucleation in the Community Atmospheric Model version 5, Atmos. Chem.
993 Phys., 14, 10411–10430, https://doi.org/10.5194/acp-14-10411-2014, 2014.

994   Westbrook, C. D. and Illingworth, A. J.: The formation of ice in a long-lived supercooled layer
995   cloud: Ice Formation in Altocumulus, Q. J. R. Meteorol. Soc., 139, 2209–2221,
996   https://doi.org/10.1002/qj.2096, 2013.

997   Wilson, T. W., Ladino, L. A., Alpert, P. A., Breckels, M. N., Brooks, I. M., Browse, J., Burrows,
998   S. M., Carslaw, K. S., Huffman, J. A., Judd, C., Kilthau, W. P., Mason, R. H., McFiggans, G.,
999   Miller, L. A., Nájera, J. J., Polishchuk, E., Rae, S., Schiller, C. L., Si, M., Vergara-Temprado, J.,
1000 Whale, T. F., Wong, J. P. S., Wurl, O., Yakobi-Hancock, J. D., Abbatt, J. P. D., Aller, J. Y.,
1001 Bertram, A. K., Knopf, D. A., and Murray, B. J.: A marine biogenic source of atmospheric ice-
1002 nucleating particles, Nature, 525, 234–238, https://doi.org/10.1038/nature14986, 2015.

1003 Winker, D. M., Tackett, J. L., Getzewich, B. J., Liu, Z., Vaughan, M. A., and Rogers, R. R.: The
1004 global 3-D distribution of tropospheric aerosols as characterized by CALIOP, Atmos. Chem.
1005 Phys., 13, 3345–3361, https://doi.org/10.5194/acp-13-3345-2013, 2013.

1006 Wu, M., Liu, X., Yu, H., Wang, H., Shi, Y., Yang, K., Darmenov, A., Wu, C., Wang, Z., Luo, T.,
1007 Feng, Y., and Ke, Z.: Understanding processes that control dust spatial distributions with global
1008 climate models and satellite observations, Atmos. Chem. Phys., 20, 13835–13855,
1009 https://doi.org/10.5194/acp-20-13835-2020, 2020.

1010 Yang, Y., Wang, H., Smith, S. J., Easter, R., Ma, P.-L., Qian, Y., Yu, H., Li, C., and Rasch, P. J.:
1011 Global source attribution of sulfate concentration and direct and indirect radiative forcing, Atmos.
1012 Chem. Phys., 17, 8903–8922, https://doi.org/10.5194/acp-17-8903-2017, 2017a.

1013 Yang, Y., Wang, H., Smith, S. J., Ma, P.-L., and Rasch, P. J.: Source attribution of black carbon
1014 and its direct radiative forcing in China, Atmos. Chem. Phys., 17, 4319–4336,
1015 https://doi.org/10.5194/acp-17-4319-2017, 2017b.

1016 Yang, Y., Wang, H., Smith, S. J., Zhang, R., Lou, S., Yu, H., Li, C., and Rasch, P. J.: Source
1017 Apportionments of Aerosols and Their Direct Radiative Forcing and Long-Term Trends Over
1018 Continental United States, Earth's Future, 6, 793–808, https://doi.org/10.1029/2018EF000859,
1019 2018.

1020 Zender, C. S., Bian, H., and Newman, D.: Mineral Dust Entrainment and Deposition (DEAD)
1021 model: Description and 1990s dust climatology, J. Geophys. Res., 108, 4416,
1022 https://doi.org/10.1029/2002JD002775, 2003.

1023 Zhang, G. J. and McFarlane, N. A.: Sensitivity of climate simulations to the parameterization of
1024 cumulus convection in the Canadian climate centre general circulation model, Atmos.-Ocean, 33,
1025 407–446, https://doi.org/10.1080/07055900.1995.9649539, 1995.

1026 Zhang, K., Wan, H., Liu, X., Ghan, S. J., Kooperman, G. J., Ma, P.-L., Rasch, P. J., Neubauer,
1027 D., and Lohmann, U.: Technical Note: On the use of nudging for aerosol–climate model
1028 intercomparison studies, Atmos. Chem. Phys., 14, 8631–8645, https://doi.org/10.5194/acp-14-
1029 8631-2014, 2014.

1030 Zhang, M., Liu, X., Diao, M., D'Alessandro, J. J., Wang, Y., Wu, C., Zhang, D., Wang, Z., and
1031 Xie, S.: Impacts of representing heterogeneous distribution of cloud liquid and ice on phase

partitioning of Arctic mixed-phase clouds with NCAR CAM5, J. Geophys. Res. Atmos., 124, 13071–13090, https://doi.org/10.1029/2019JD030502, 2019.

Zhang, M., Xie, S., Liu, X., Lin, W., Zhang, K., Ma, H.-Y., Zheng, X., and Zhang, Y.: Toward understanding the simulated phase partitioning of Arctic single-layer mixed-phase clouds in E3SM, Earth Space Sci., 7, e2020EA001125, https://doi.org/10.1029/2020EA001125, 2020.

Zhang, Y., Xie, S., Lin, W., Klein, S. A., Zelinka, M., Ma, P., Rasch, P. J., Qian, Y., Tang, Q., and Ma, H.: Evaluation of clouds in version 1 of the E3SM atmosphere model with satellite simulators, J. Adv. Model. Earth Syst., 11, 1253–1268, https://doi.org/10.1029/2018MS001562, 2019.

Zhao, X. and Liu, X.: Global Importance of Secondary Ice Production, Geophys. Res. Lett., 48, e2021GL092581, https://doi.org/10.1029/2021GL092581, 2021.

Zhao, X., Liu, X., Burrows, S. M., and Shi, Y.: Effects of marine organic aerosols as sources of immersion-mode ice-nucleating particles on high-latitude mixed-phase clouds, Atmos. Chem. Phys., 21, 2305–2327, https://doi.org/10.5194/acp-21-2305-2021, 2021a.

Zhao, X., Liu, X., Phillips, V. T. J., and Patade, S.: Impacts of secondary ice production on Arctic mixed-phase clouds based on ARM observations and CAM6 single-column model simulations, Atmos. Chem. Phys., 21, 5685–5703, https://doi.org/10.5194/acp-21-5685-2021, 2021b.

1051   **Table 1.** Experiments conducted in this study.

Experiment	Description
CTRL	Control simulation using the CNT parameterization for heterogeneous ice nucleation and Kok et al. (2014a, b) for dust emission parameterization.
noArc	Same as CTRL, but turn off heterogeneous ice nucleation in mixed-phase clouds by HLD.
noNAf	Same as CTRL, but turn off heterogeneous ice nucleation in mixed-phase clouds by North African dust.
noEAs	Same as CTRL, but turn off heterogeneous ice nucleation in mixed-phase clouds by East Asian dust.

1052

Table 2. Annual and seasonal mean Arctic dust burden (mg m^{-2}) from different sources. The numbers in parentheses are the relative contributions (%) of each source to the total Arctic dust burden. The total Arctic dust burden is shown in the last row.

	ANN	MAM	JJA	SON	DJF
Arc	2.1 (30.7)	0.3 (3.9)	5.1 (50.4)	2.5 (47.5)	0.5 (14.6)
NAm	0.1 (0.9)	0.1 (1.3)	0.1 (0.6)	0.0 (0.7)	0.0 (1.2)
NAf	1.7 (24.2)	3.7 (41.4)	1.5 (14.4)	0.7 (12.9)	0.9 (26.4)
CAs	0.9 (12.8)	1.1 (12.5)	1.3 (13.0)	0.8 (14.7)	0.3 (10.1)
MSA	0.8 (11.5)	1.6 (17.9)	0.7 (7.0)	0.3 (6.1)	0.6 (17.4)
EAs	1.4 (19.9)	2.0 (23.0)	1.5 (14.7)	0.9 (18.1)	1.0 (30.2)
RoW	0.0 (0.0)	0.0 (0.0)	0.0 (0.0)	0.0 (0.0)	0.0 (0.1)
Total Burden (mg m^{-2})	6.9	8.9	10.2	5.2	3.3

1057   **Table 3.** Summary of the nine Arctic INP measurements used for INP comparisons in Figure 8.

	Location	Time period	Measured platform	Reference	Possible INP source mentioned in literature	INP source attribution from modeling[+]
A	Utqiaġvik	Apr. 2008 (spring)	Aircraft	McFarquhar et al. (2011)	Metallic or composed of dust[*]	LLD (EAs)
B	Alert	Mar. - May 2014 (spring)	Ground-based	Mason et al. (2016)	Not mentioned	LLD (EAs)
C	Alert	Mar. 2016 (spring)	Ground-based	Si et al. (2019)	LLD from Gobi Desert	LLD (EAs)
D	Zeppelin	Mar. 2017 (spring)	Ground-based	Tobo et al. (2019)	Marine organic aerosols	HLD (NEu)
E	Oliktok Point	Mar. - May 2017 (spring)	Ground-based	Creamean et al. (2018)	Dust and primary marine aerosols	LLD (mainly from EAs and some from NAf)
F	Alert	Jun. - Jul. 2014 (summer)	Ground-based	Mason et al. (2016)	Not mentioned	HLD (NCa)
G	Zeppelin	Jul. 2016 (summer)	Ground-based	Tobo et al. (2019)	HLD from Svalbard or other high latitude sources[**]	HLD (NEu)
H	Utqiaġvik	Oct. 2004 (autumn)	Aircraft	Prenni et al. (2007)	Dust and carbonaceous particles	HLD (NCa) and LLD (EAs)
I	South of Iceland	Oct. 2014 (autumn)	Aircraft	Sanchez-Marroquin et al. (2020)	Icelandic dust	Dominated by HLD (GrI), little from LLD (NAf)

1058   [+] The modeling analyses include INP contribution from HLD (using SM20), LLD (using D15),
1059   BC, and SSA. The
1060   [*] Carbonate, black carbon, and organic may also contribute, according to Hiranuma et al. (2013).
1061   [**] The HLD in this campaign is reported to have remarkably high ice nucleating ability, which
1062   may be related to the presence of organic matter.
1063

1064 **Table 4.** Arctic averaged surface downwelling radiative fluxes and TOA cloud radiative forcing
1065 changes caused by dust INPs originated from local Arctic sources (Arc), North Africa (NAf), and
1066 East Asia (EAs). Units are W m^{-2}.

	ANN			MAM			JJA			SON			DJF		
	SW	LW	Net	SW	LW	Net	SW	LW	Net	SW	LW	Net	SW	LW	Net
Part 1. INP effect on surface downwelling radiative fluxes															
Arc	0.11	-0.36	-0.24	0.27	-0.31	-0.03	0.12	0	0.12	0.04	-0.55	-0.51	0.02	-0.56	-0.54
NAf	0.33	-0.25	0.08	0.78	-0.60	0.19	0.50	0.01	0.51	0.02	-0.03	-0.02	0.03	-0.39	-0.36
EAs	0.35	-0.41	-0.06	0.68	-0.60	0.09	0.59	0.02	0.61	0.08	-0.27	-0.19	0.04	-0.80	-0.76
Part 2. INP effect on TOA cloud radiative forcing															
Arc	0.06	-0.11	-0.05	0.06	-0.07	-0.01	0.14	-0.02	0.12	0.03	-0.23	-0.20	0.01	-0.12	-0.11
NAf	0.20	-0.23	-0.03	0.34	-0.34	0	0.41	-0.18	0.24	0.03	-0.20	-0.16	0.02	-0.23	-0.21
EAs	0.20	-0.24	-0.04	0.22	-0.23	-0.02	0.46	-0.17	0.29	0.09	-0.29	-0.20	0.02	-0.26	-0.24

1067

45
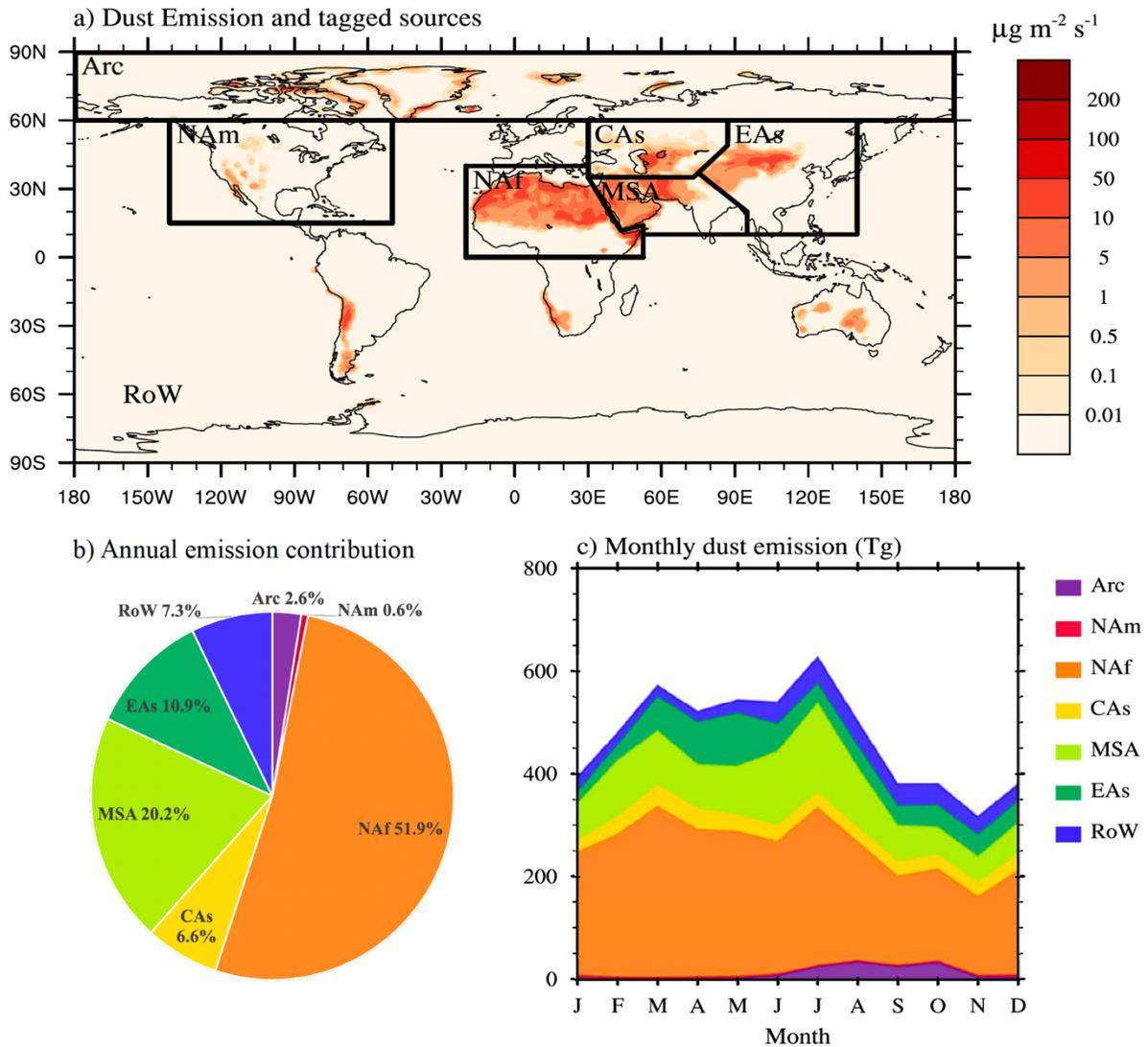
Figure 1. a) Simulated global annual mean dust emission with 7 tagged source regions (Arc: Arctic; NAm: North America; NAf: North Africa; CAs: Central Asia; MSA: Middle East and South Asia; EAs: East Asia; RoW: Rest of the World). b) The respective percentage contributions to the global annual mean dust emission from the individual source regions. c) Seasonal cycle of global dust emission.
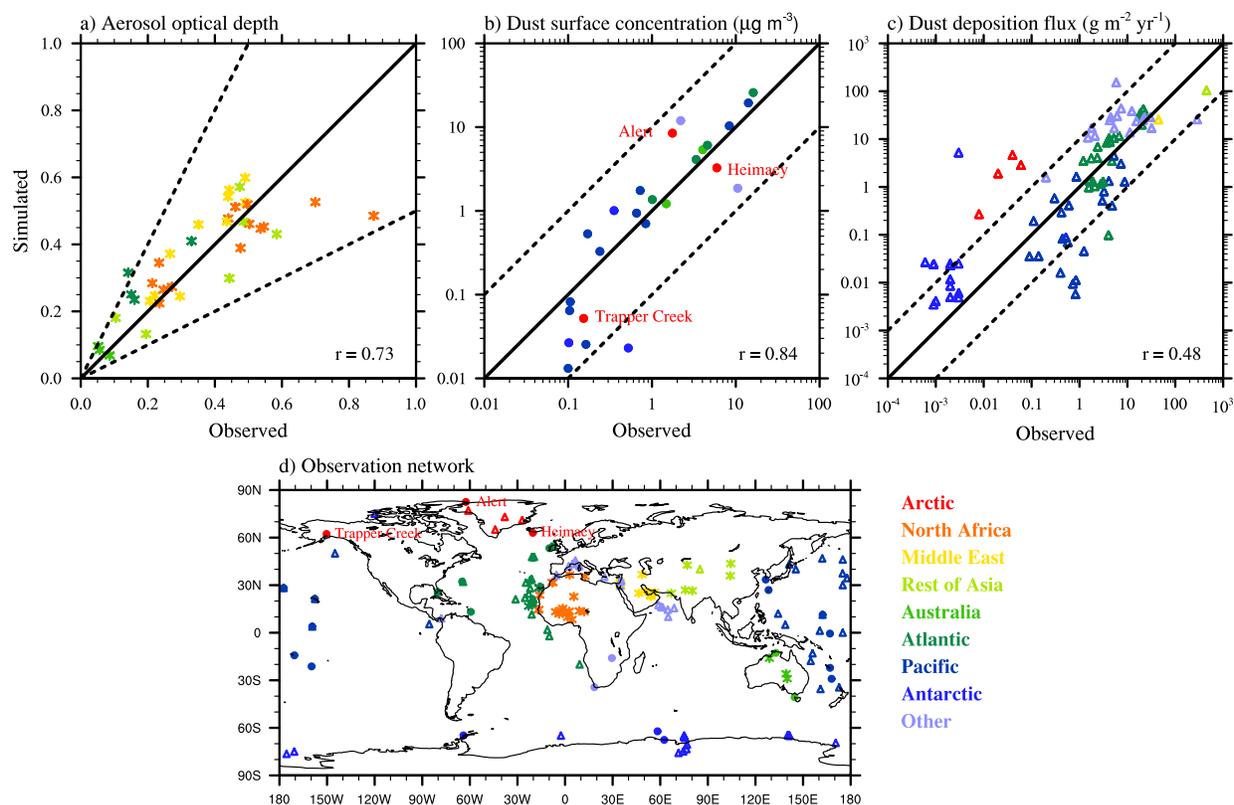
Figure 2. Comparison of observed and simulated a) averaged AOD at 40 dust-dominated stations (stars), b) dust surface concentration at 25 sites (circles), and c) dust deposition flux at 84 sites (triangles). Solid lines represent 1:1 comparison. Dashed lines mark 2 factor of magnitude bias in panel a) and 1 order of magnitude differences in panel b) and c). For each comparison, the correlation coefficient (r) is noted. The AOD data is conducted by AERONET. The dust surface concentration measurements include 20 stations managed by Rosenstiel School of Marine and Atmospheric Science at the University of Miami (Prospero et al., 1989; Prospero, 1996; Arimoto et al., 1995), two Australia stations (Maenhaut et al., 2000a, b), and three Arctic stations (Heimaey (Prospero et al., 2012), Alert (Sirois and Barrie, 1999), and Trapper Creek (IMPROVE)). The deposition fluxes data is a compilation of measurements from Ginoux et al. (2001), Mahowald et al. (2009), and the Dust Indicators and Records in Terrestrial and Marine Paleoenvironments (DIRTMAP) database (Tegen et al., 2002; Kohfeld and Harrison, 2001). Stations are grouped regionally and classified by different colors. The locations of the measurements are shown in panel d).

47
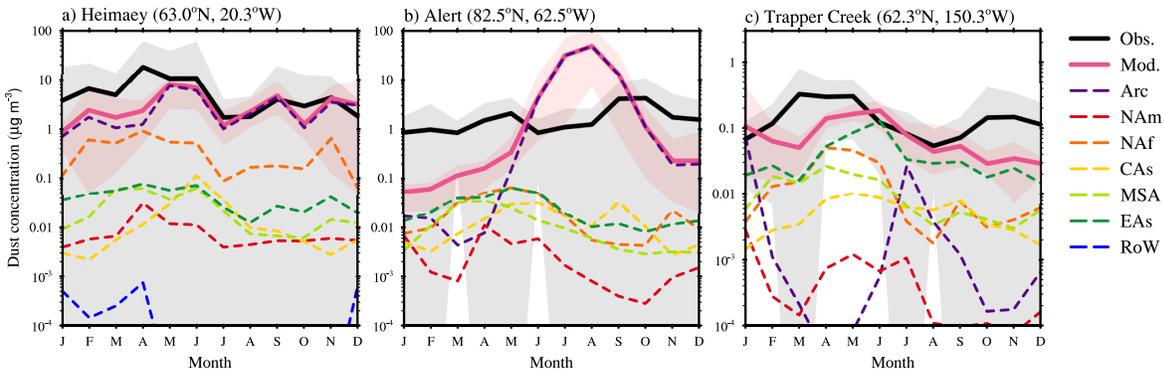
1090

Figure 3. Comparison of measured (black solid line, with gray shade representing standard deviation) and simulated (pink solid line, with pink shade representing year-to-year variability) monthly mean dust surface concentration at three high latitude stations – a) Heimaey, b) Alert, and c) Trapper Creek. The model results are averaged from year 2007 to 2011. Contributions from seven tagged sources are shown by colored dashed lines. The locations of the three stations are shown in Figure 2d. The measurements at Heimaey (Prospero et al., 2012), Alert (Sirois and Barrie, 1999), and Trapper Creek (IMPROVE) are averaged for the years 1997 to 2002, 1980 to 1995, and 2007 to 2011, respectively. The dust concentrations at Trapper Creek only include particles with diameter less than 2.5 μm. The other two stations include dust over the whole size range.

1101
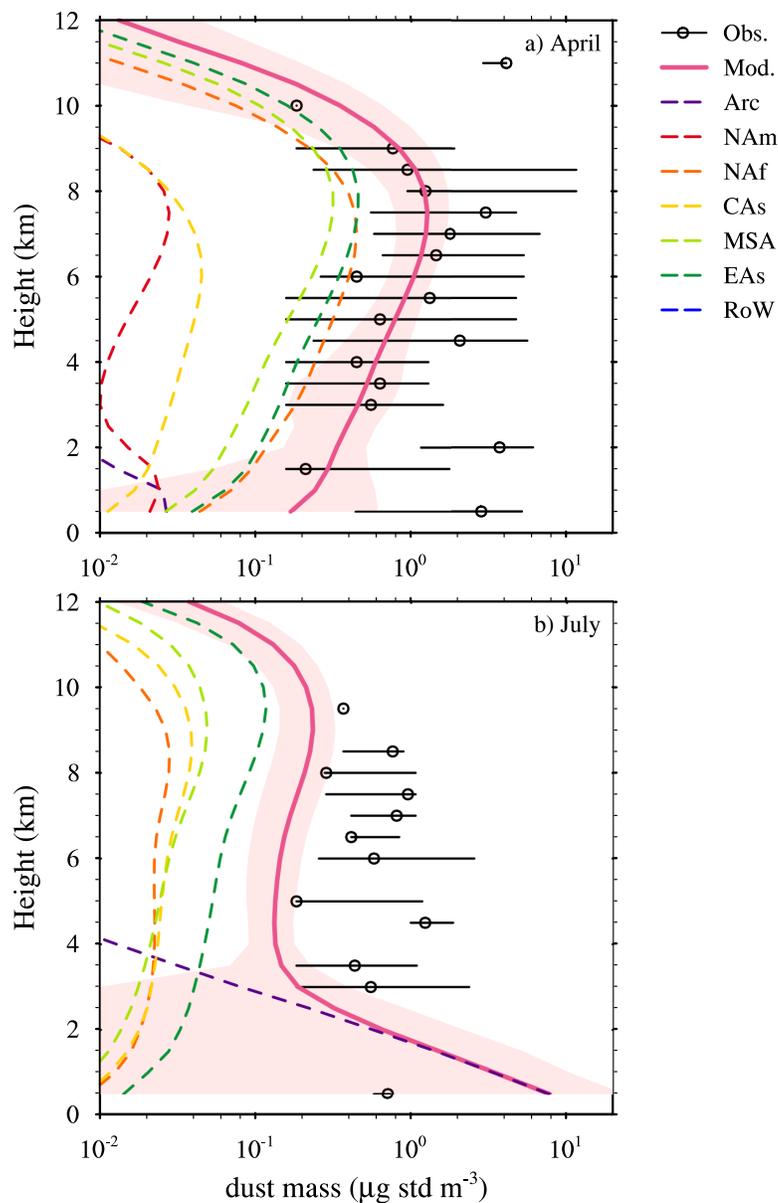
Figure 4. Comparison of vertical dust concentrations from ARCTAS flight observations (Jacob et al., 2010) (black circle) and CTRL simulation (pink solid line) in a) April and b) July. We show median values for observations at each level. The maximum and minimum of the measurements at each level are shown by black lines. Contributions from the seven tagged sources in CTRL are shown by colored dashed lines. The ARCTAS dust mass concentrations are derived from measured calcium and sodium concentrations. The measurements data are processed using the same method as Breider et al. (2020). Briefly, we assume a calcium to dust mass ratio of 6.8% and further correct the calcium concentrations for sea salt by assuming a calcium to sodium ratio of 4%. Only measurements obtained north of 60°N are used for the analyses. The low-altitude observations near Fairbanks, Barrow, and Prudhoe Bay are removed.

1113   Also, data from below 1 km on 1, 4, 5, 9 July is removed to exclude the influence of wildfire.
1114   The ARCTAS flight campaign was conducted in 2008, while the modeled vertical profiles are
1115   averaged for each April and July from 2007 to 2011, respectively. Following Groot Zwaaftink et
1116   al. (2016), the simulation profiles are averaged for the regions north of 60°N and 170°W to
1117   35°W in April and 135°W to 35°W in July. Also, the observations have a cut-off size of 4 μm
1118   and thus is only compared with simulated dust concentrations in the same size range. The pink
1119   shade on each panel represents the standard deviation with respect to time and space for the
1120   simulated total dust concentrations.

1121
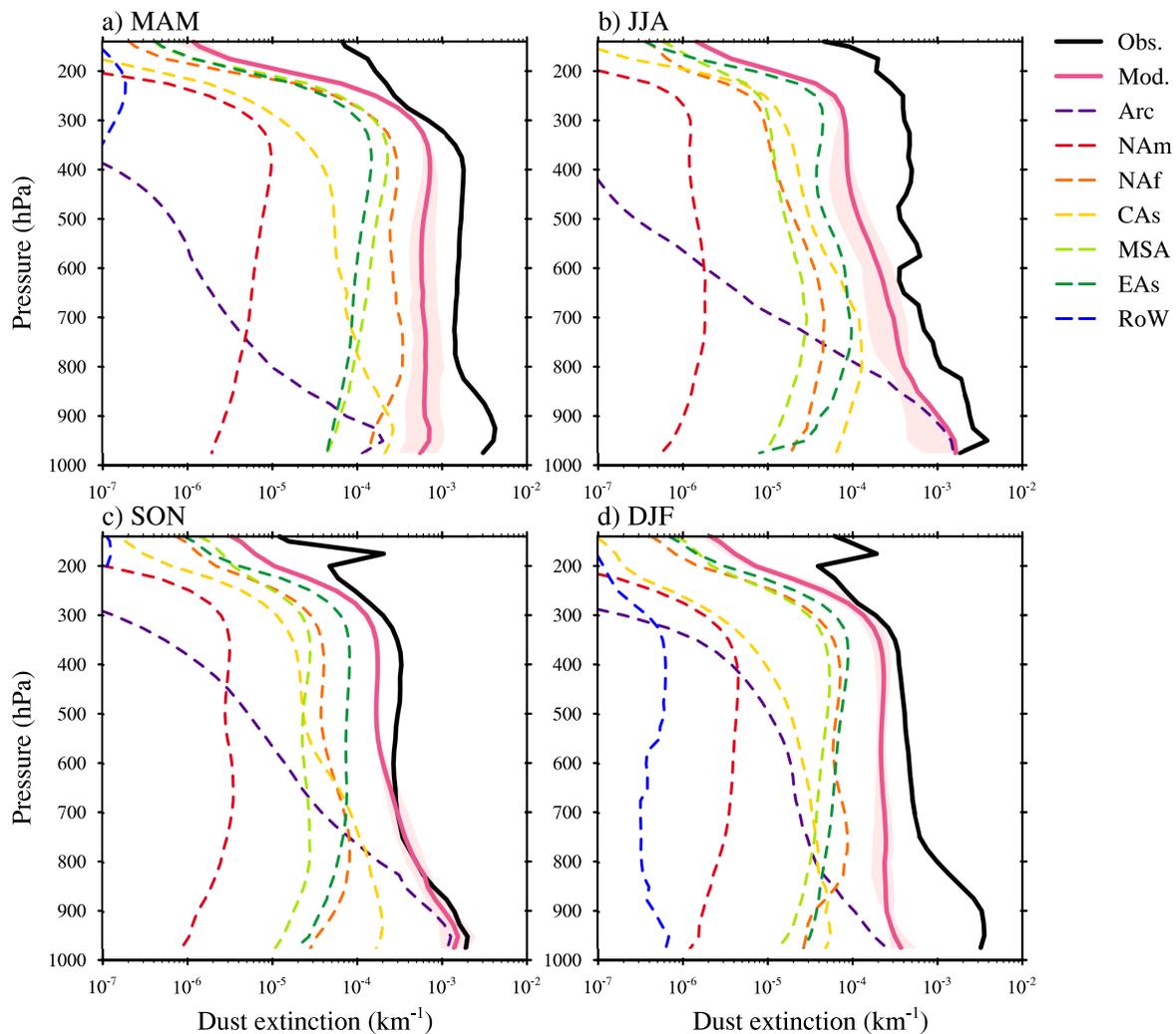
1122

Figure 5. Comparison of seasonal CALIPSO retrieved (Luo et al., 2015a, b) (black solid line) and model simulated (pink solid line; with pink shade representing year-to-year variability) dust extinction vertical profiles in the Arctic. Contributions from seven tagged sources are shown by colored dashed lines. The CALIPSO retrieval is for the year 2007 to 2009, while the model is averaged over the same years.
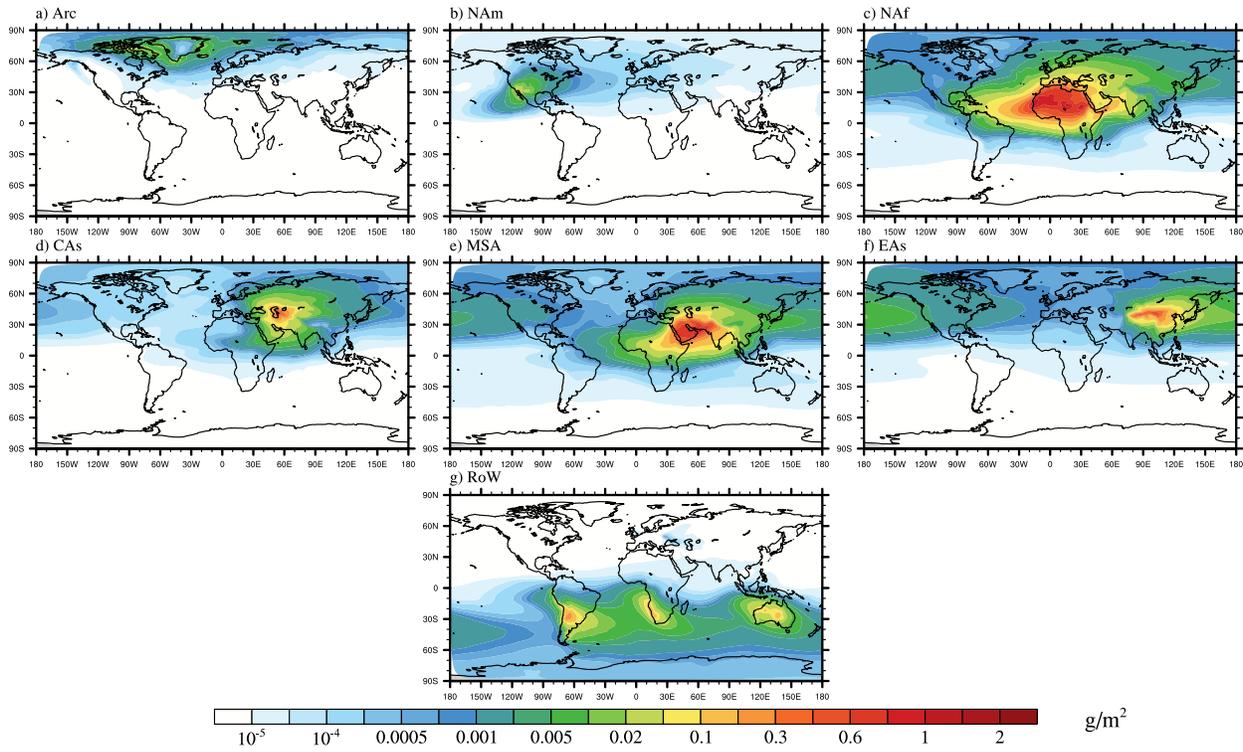
1128

Figure 6. Spatial distribution of annual mean (year 2007 to 2011) dust column burdens for various tagged sources.
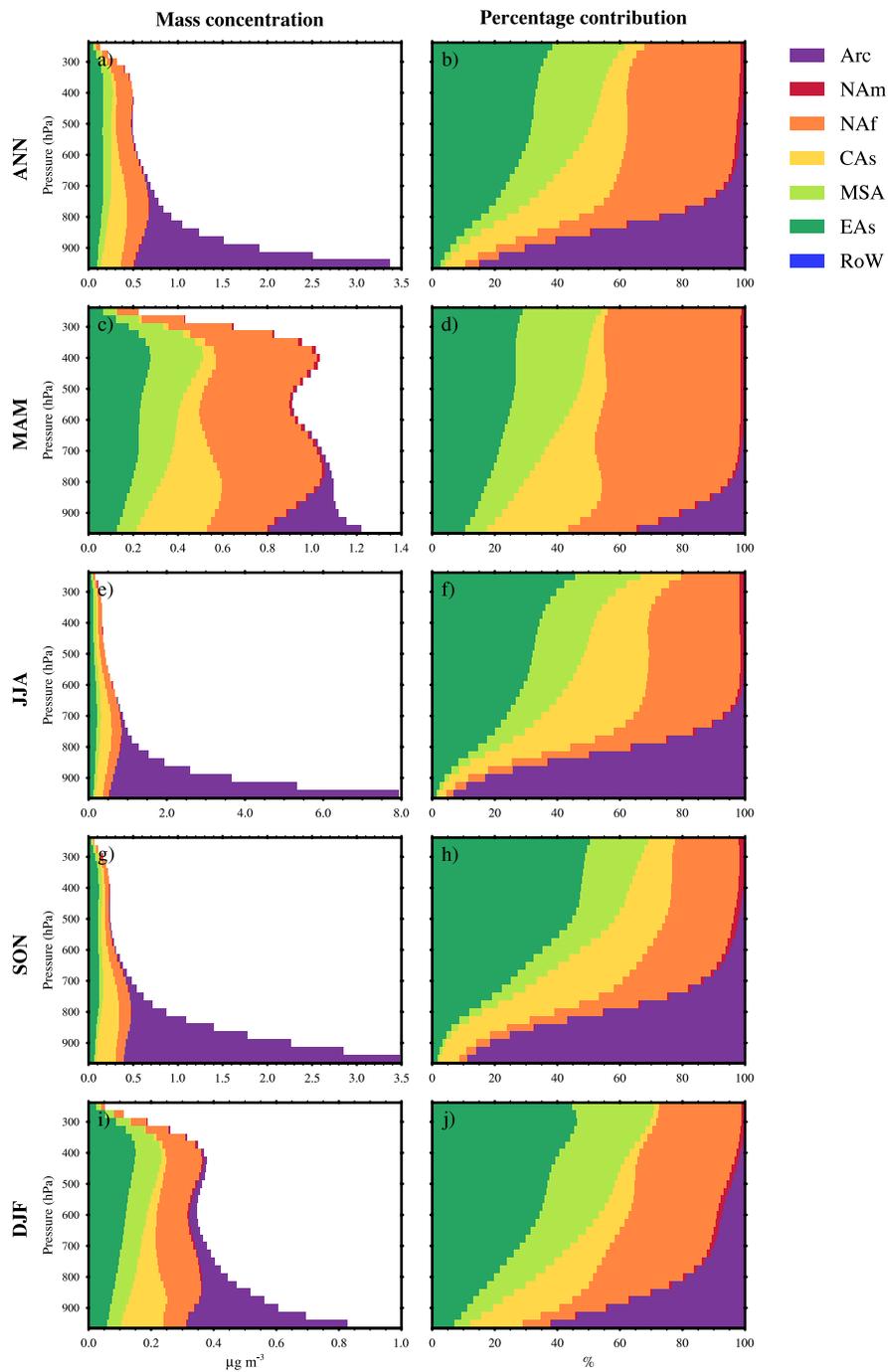
1131

Figure 7. Annual and seasonal mean (year 2007 to 2011) Arctic vertical dust concentrations (left panel) and percentage contributions from tagged sources (right panel). Different tagged sources are classified by different colors.
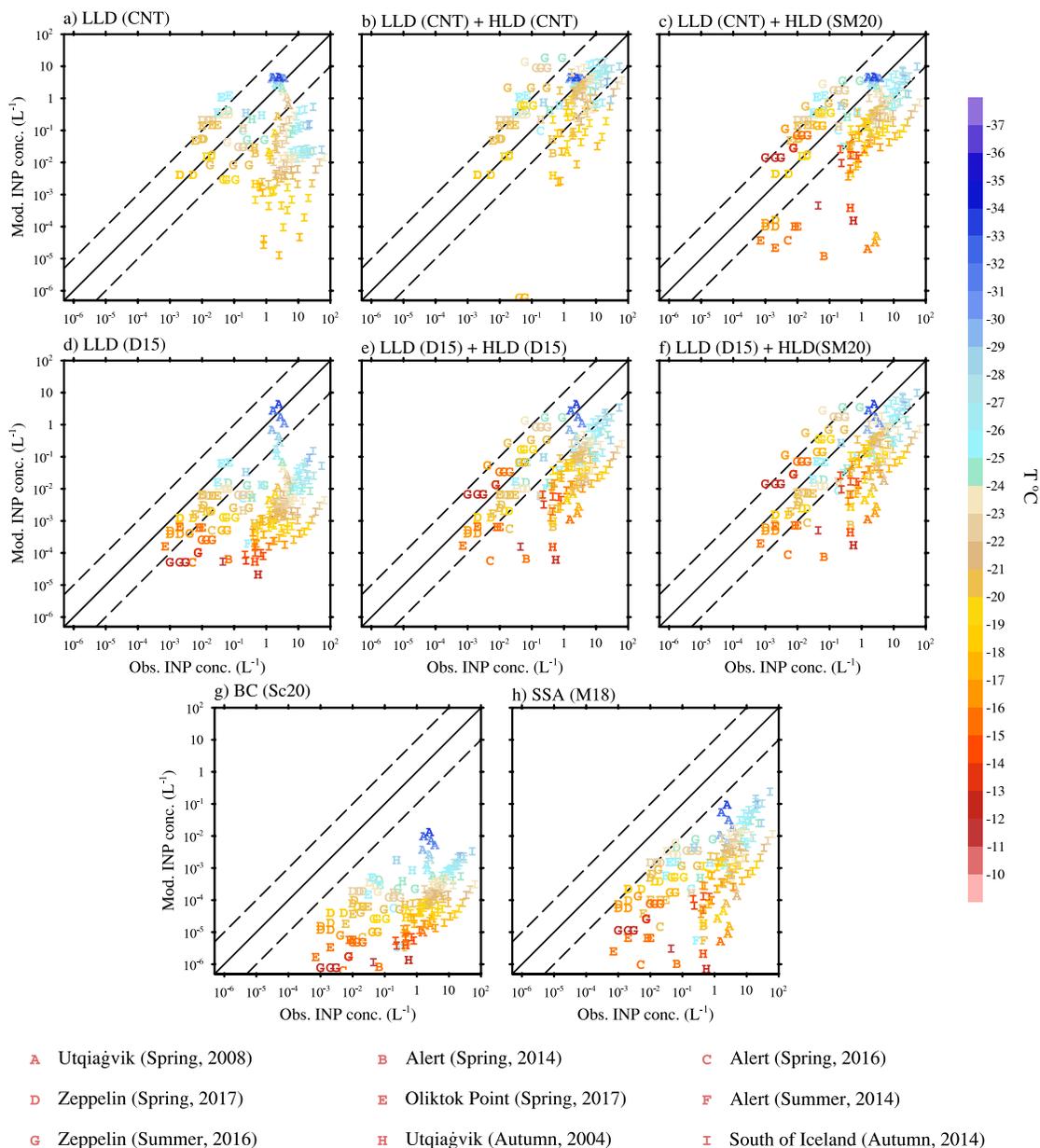
Figure 8. Comparison of predicted versus observed INP concentrations in the Arctic. The predicted INP concentrations are derived from a) LLD using classical nucleation theory (CNT), b) LLD and HLD, both using CNT, c) LLD using CNT and HLD using Sanchez-Marroquin et al (2020; SM20), c) LLD using DeMott et al. (2015; D15), d) LLD and HLD, both using D15, e) LLD using D15 and HLD using SM20, f) BC using Schill et al. (2020; Sc20), and g) SSA using McCluskey et al. (2018; M18). SSA includes both marine organic aerosol and sea salt. Nine INP datasets are classified by symbol "A" to "I", the color of which represents the temperature reported in the observations. The observations for datasets "A", "C", "E", "H" are monthly mean values. Samples for datasets "D", "G", "I" are selected randomly and only 15% of them are plotted. Details of each campaign are summarized in Table 3. The modelled INP concentrations

1146 are diagnosed using the observed temperatures and monthly averaged aerosol properties of the
1147 corresponding month from year 2007 to 2011. The INP concentrations for CNT are defined as
1148 the CNT immersion freezing rate integrated by 10 s, following Hoose et al. (2010) and Wang et
1149 al. (2014). Solid line in each panel represents 1:1 comparison, while dashed lines outline one
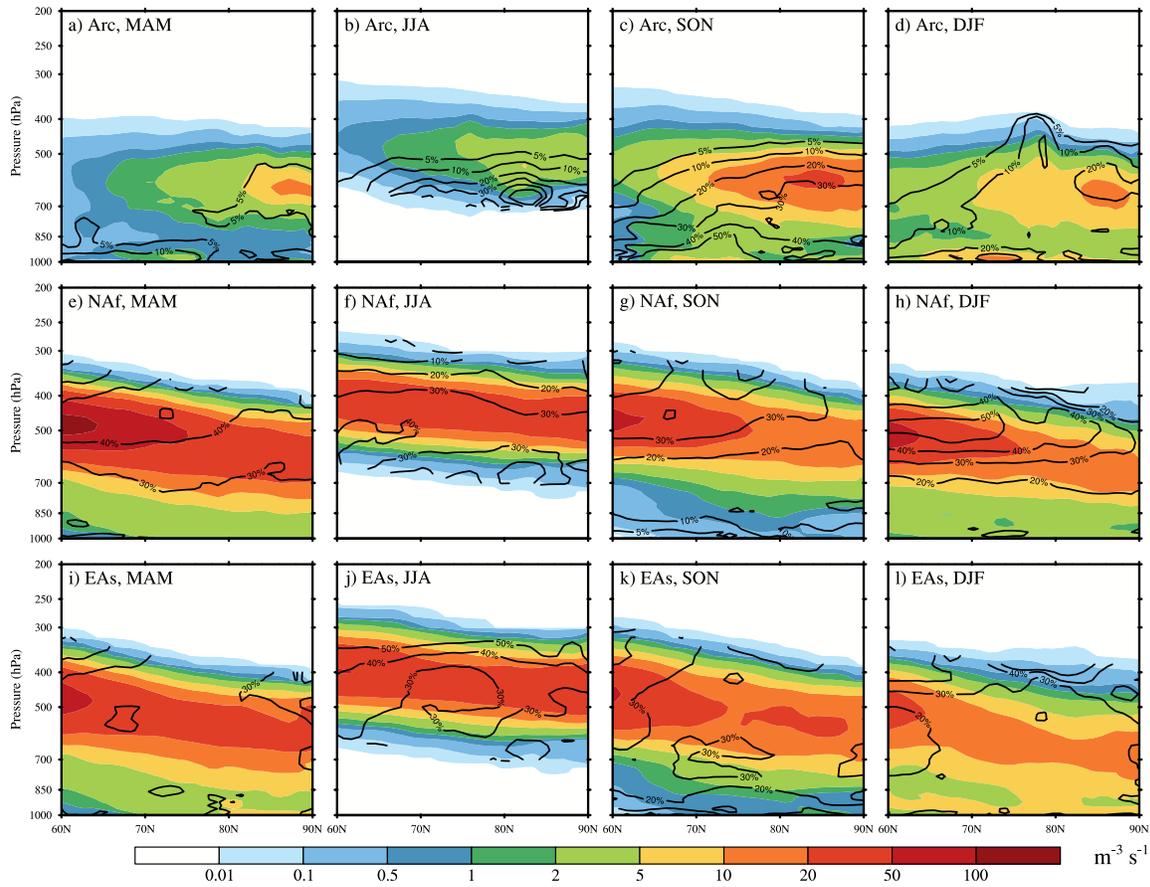1150 order of magnitude differences. The unit for INP concentration is L^{-1}.

1151
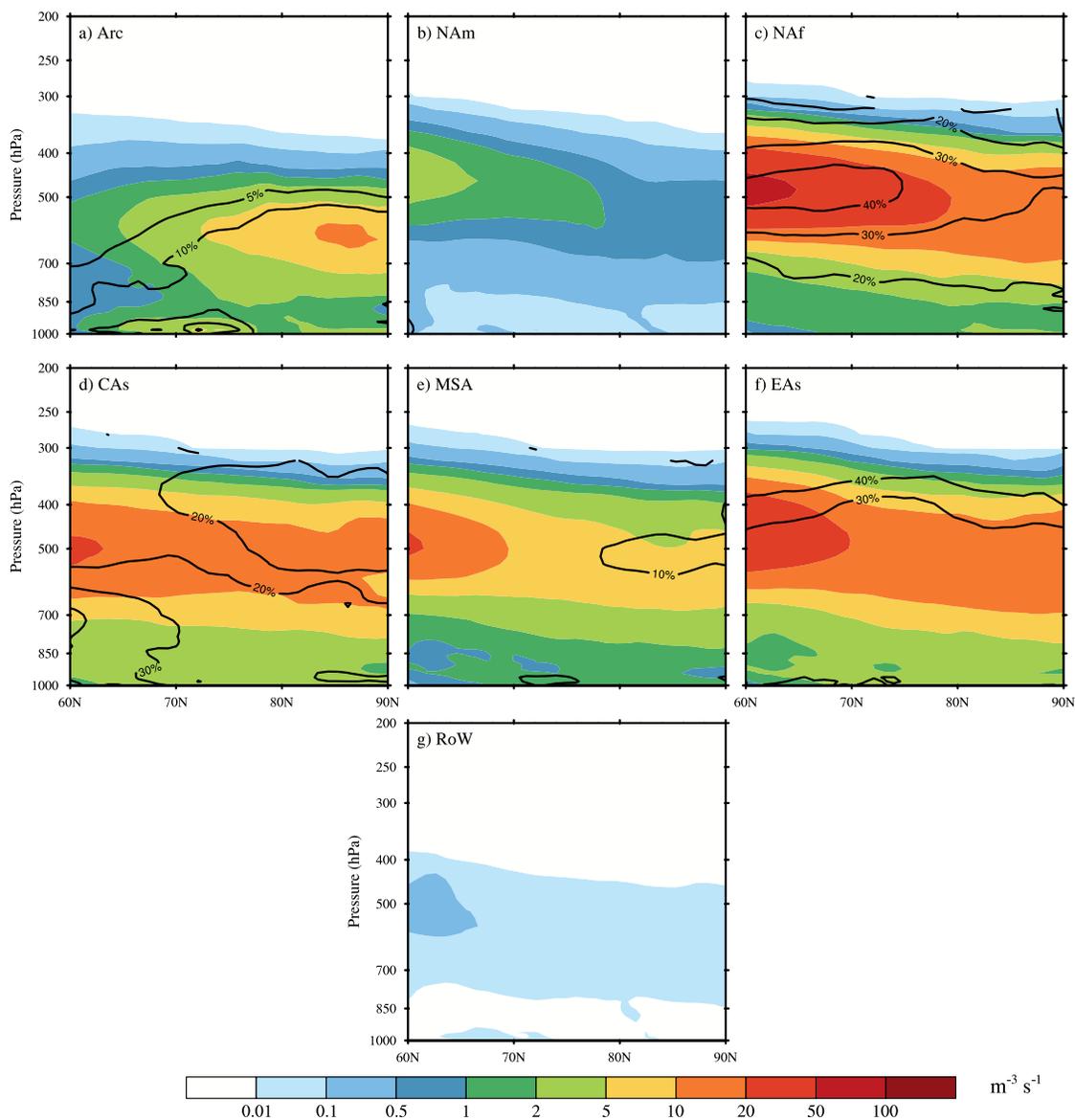
Figure 9. Annual and zonal mean (year 2007 to 2011) ambient mixed-phase cloud immersion freezing rates (unit: m^{-3} s^{-1}) in the Arctic (60-90°N) for the seven dust sources. Black contours are the percentage contributions from each dust source to the total immersion freezing rate.

Figure 10. Seasonal variations (year 2007 to 2011) of the mixed-phase clouds immersion freezing rates (unit: $m^{-3} s^{-1}$) over the Arctic for dust emitted from the Arctic (top panel), North Africa (middle panel), and East Asia (bottom panel). Black contours are the percentage contributions from each dust source to the total immersion freezing rate in the corresponding season.
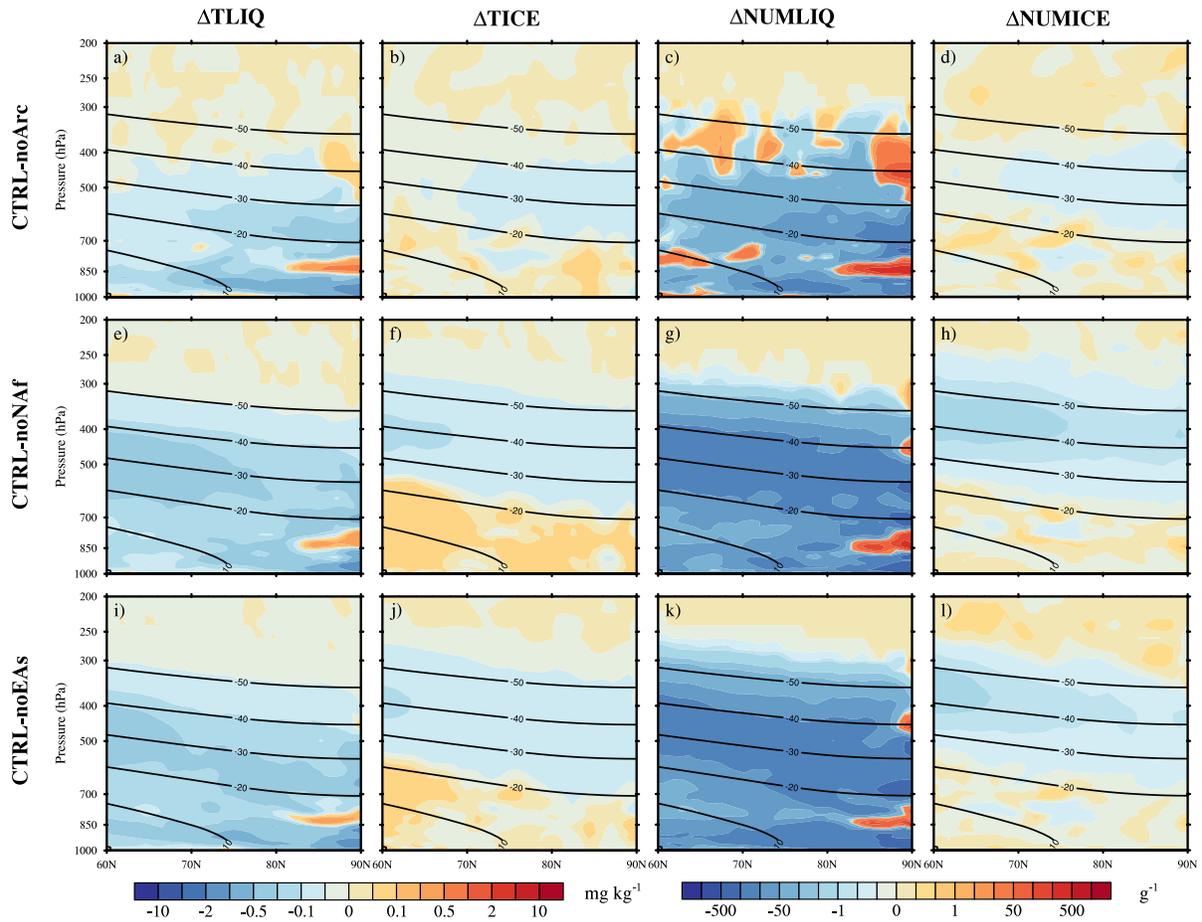
1164

Figure 11. Annual and zonal mean differences (year 2007 to 2011) in total liquid water mass mixing ratio (TLIQ), total ice mixing ratio (TICE), cloud droplet number concentration (NUMLIQ), and cloud ice number concentration (NUMICE) in the Arctic. Black contours are zonal averaged temperatures in °C. Top, middle, and bottom panels show the differences between CTRL and noArc, noNAf, and noEAs, respectively.
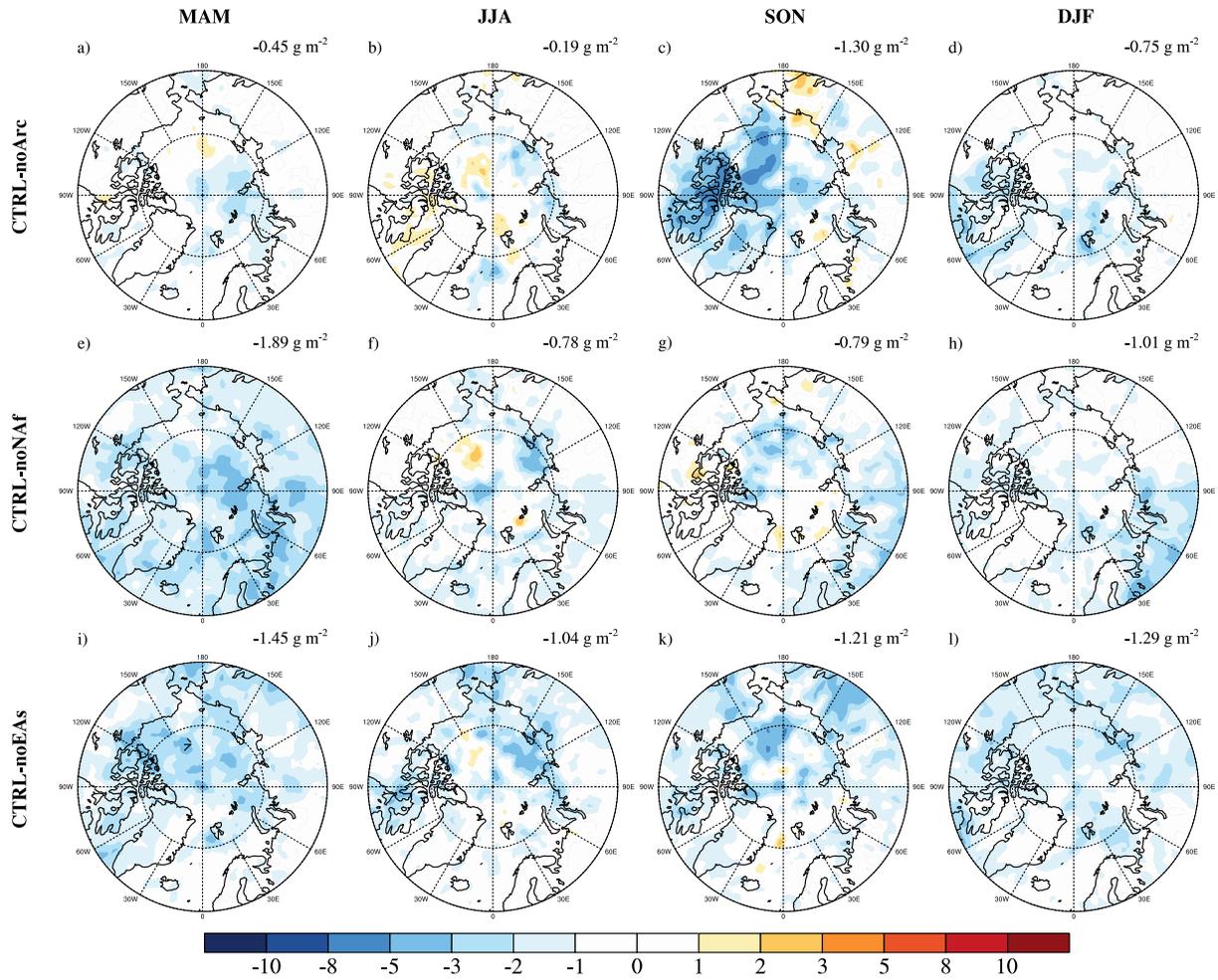
Figure 12. Seasonal changes (year 2007 to 2011) in LWP (unit: g m^{-2}) caused by dust INPs from the Arctic (top panel), North Africa (middle panel), and East Asia (bottom panel). The numbers are averaged LWP differences in the Arctic.
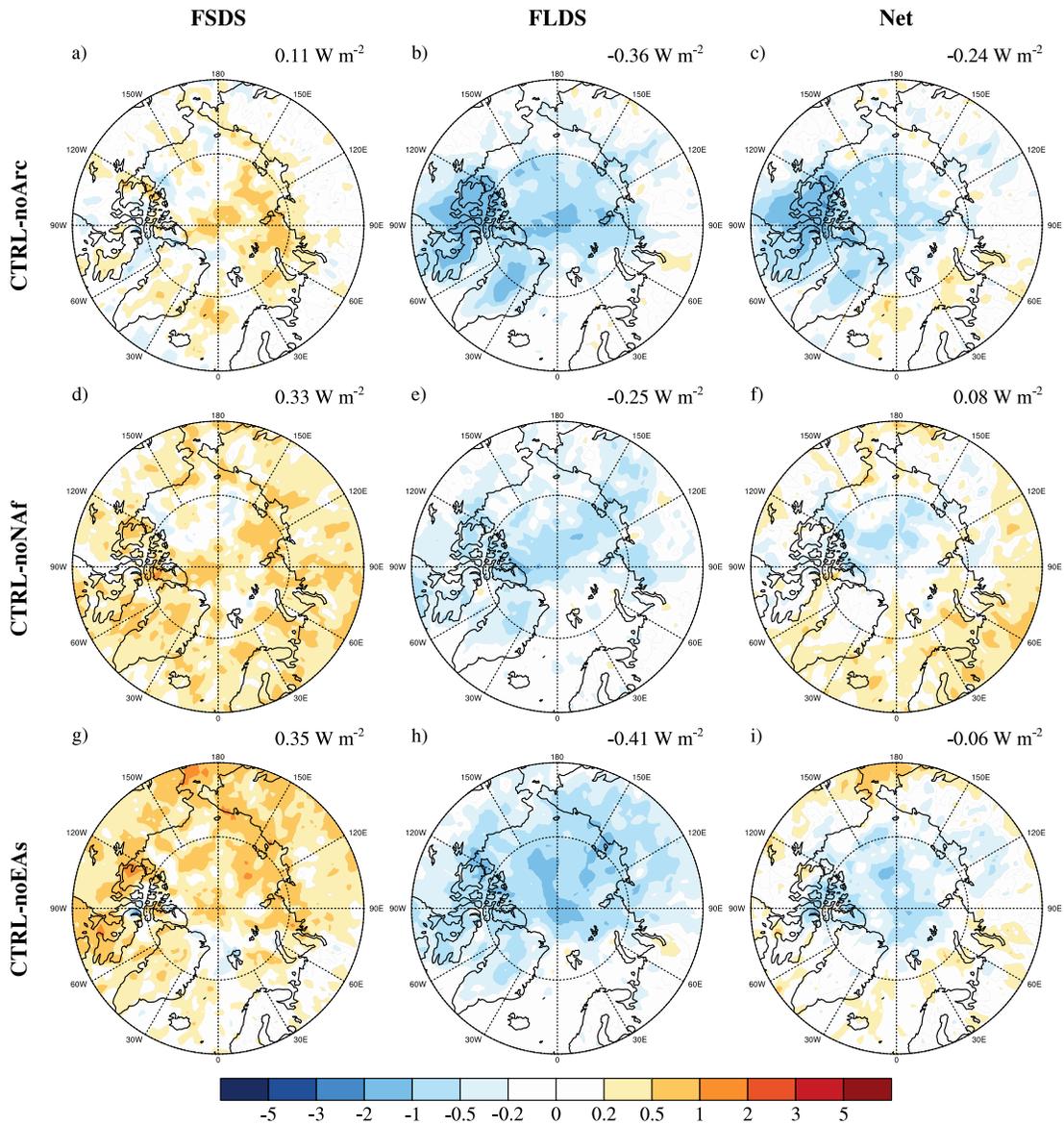
Figure 13. Changes in annual mean (year 2007 to 2011) downwelling radiative fluxes at the surface (unit: W m⁻²) caused by dust INPs from the Arctic (top panel), North Africa (middle panel), and East Asia (bottom panel). Left, middle, and right panels are downwelling shortwave (FSDS), longwave (FLDS), and net (FSDS + FLDS) radiative fluxes, respectively. The numbers are averaged radiative flux differences in the Arctic.

1182
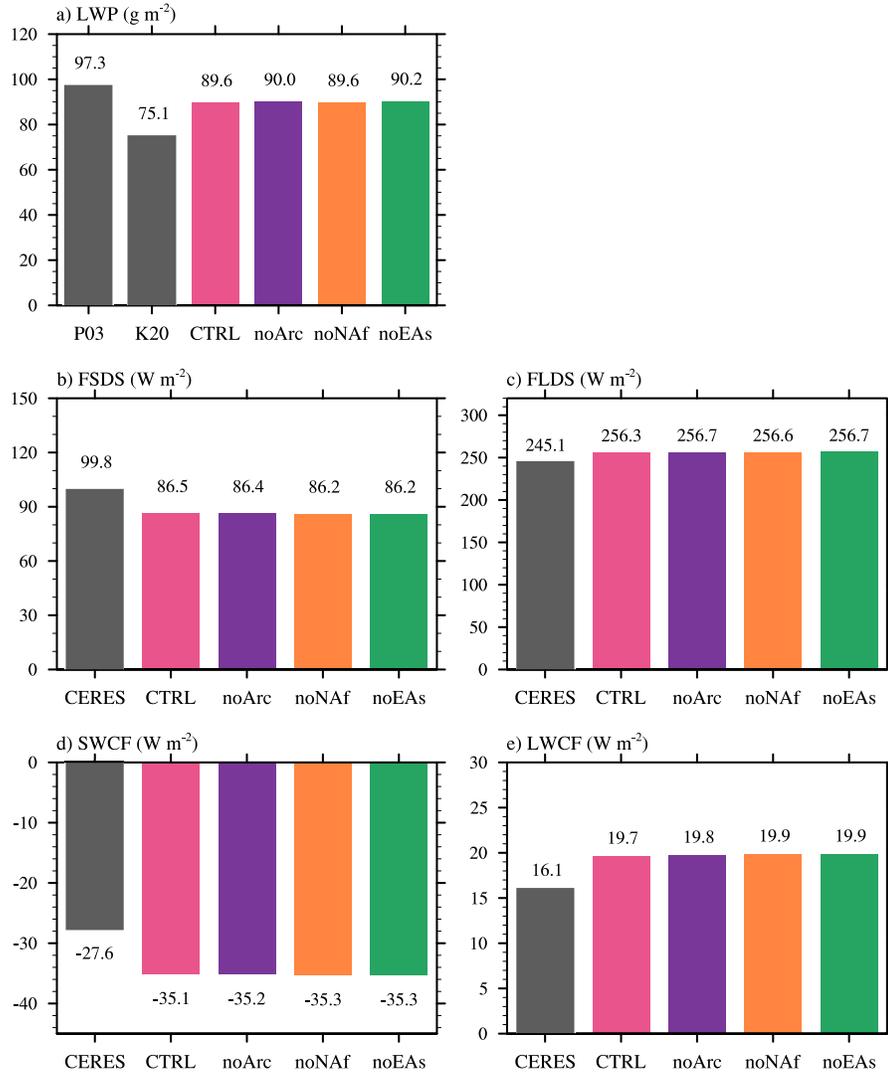
Figure 14. a) Annual mean Arctic averaged LWP over ocean for the MODIS observations (2007-2009) and the four simulations (2007-2008). Two MODIS datasets are used, including the standard product (Platnick et al., 2003; P03) and an improved one (Khanal et al., 2020; K20). The MODIS simulator is used to calculate the simulated LWP. b) - e) Annual mean Arctic averaged b) FSDS, c) FLDS, d) SWCF, and e) LWCF for the CERES observation (2007-2011) and the four simulations (2007-2011).

1189